

Recruitment of Parvalbumin-Positive Interneurons Determines Hippocampal Function and Associated Behavior

Elke C. Fuchs,¹ Aleksandar R. Zivkovic,¹ Mark O. Cunningham,² Steven Middleton,² Fiona E.N. LeBeau,² David M. Bannerman,³ Andrei Rozov,¹ Miles A. Whittington,² Roger D. Traub,⁴ J. Nicholas P. Rawlins,³ and Hannah Monyer^{1,*}

¹Department of Clinical Neurobiology, University Hospital of Neurology, IZN, Im Neuenheimer Feld 364, 69120 Heidelberg, Germany

²School of Neurology, Neurobiology and Psychiatry, University of Newcastle, Newcastle NE2 4HH, United Kingdom

³Department of Experimental Psychology, University of Oxford, South Parks Road, Oxford, OX1 3UD, United Kingdom

⁴Departments of Physiology and Pharmacology and Neurology, State University of New York, Downstate Medical Center, 450 Clarkson Avenue, Box 31, Brooklyn, NY 11203, USA

*Correspondence: monyer@urz.uni-hd.de

DOI 10.1016/j.neuron.2007.01.031

SUMMARY

Perisomatic inhibition provided by a subgroup of GABAergic interneurons plays a critical role in timing the output of pyramidal cells. To test their contribution at the network and the behavioral level, we generated genetically modified mice in which the excitatory drive was selectively reduced either by the knockout of the GluR-D or by conditional ablation of the GluR-A subunit in parvalbumin-positive cells. Comparable cell type-specific reductions of AMPA-mediated currents were obtained. Kainate-induced gamma oscillations exhibited reduced power in hippocampal slices from *GluR-D*^{-/-} and *GluR-A*^{PVCre-/-} mice. Experimental and modeling data indicated that this alteration could be accounted for by imprecise spike timing of fast-spiking cells (FS) caused by smaller interneuronal EPSPs. *GluR-D*^{-/-} and *GluR-A*^{PVCre-/-} mice exhibited similar impairments in hippocampus-dependent tasks. These findings directly show the effects of insufficient recruitment of fast-spiking cells at the network and behavioral level and demonstrate the role of this subpopulation for working and episodic-like memory.

INTRODUCTION

GABAergic interneurons are the main source of inhibition in the brain, but in addition there is increasing evidence for their pivotal role in synchronous network activity. GABAergic interneurons can phase the output of pyramidal cells, giving rise to oscillatory activity in different fre-

quency bands (Cobb et al., 1995; Tamas et al., 2000; Whittington et al., 1995; Ylinen et al., 1995a; Ylinen et al., 1995b). This form of network activity is associated with a number of cognitive functions and plasticity in the brain (Engel et al., 2001; Gray et al., 1989; Singer, 1993).

Numerous anatomical, electrophysiological, and molecular studies have identified features of GABAergic interneurons that enable this cell population to control network activity (Buzsaki et al., 2004; McBain and Fisahn, 2001). Thus, extensive axonal arborization permits most GABAergic interneurons to control the activity of large neuronal ensembles (Freund and Buzsaki, 1996; Pawelzik et al., 2002). Expression studies identified a number of genes that are predominantly or exclusively expressed in GABAergic interneurons (Tansey et al., 2002). Although not entirely satisfactory and comprehensive, some of their unique features have served to classify GABAergic neurons (Markram et al., 2004; McBain and Fisahn, 2001; Yuste, 2005).

Considering the heterogeneity of GABAergic interneurons, an obvious question arises as to their functional role in vivo. Of all GABAergic interneuron subgroups, cells expressing the Ca²⁺ buffer parvalbumin (PV) are certainly among the most and best studied. This is in part due to their prevalence—they comprise about 20% of the total GABAergic population and are hence more numerous compared to other subtypes. Also, the availability of specific antibodies (Celio et al., 1988) has been of great value for anatomical studies that revealed the axonal arborization pattern of this cell population and showed that many of them preferentially target the perisomatic compartment of other neurons (Katsumaru et al., 1988; Ribak et al., 1990). Finally, the finding that PV-positive cells were characterized by a fast-spiking action potential pattern upon depolarization (Kawaguchi et al., 1987) was of great importance, and many electrophysiological studies relied on this spiking pattern that became the signature of this cell class. It was this feature that allowed their

identification in the acute slice preparation and that, in combination with molecular studies, led to the identification of genes. Although it is well known that alteration of inhibition has profound effects at the network level, it is surprising that only few attempts have been made so far to alter the function of GABAergic interneurons in general or of certain subsets in particular (Joho et al., 1999; Vreugdenhil et al., 2003).

Mice with altered glutamate receptors and hence changed excitability have proved to be valuable models to study different forms of learning and plasticity in vitro and in vivo. Thus, specific knockouts of NMDA or AMPA receptor subunits were shown to be associated with altered plasticity and learning (Reisel et al., 2002; Tsien et al., 1996; Zamanillo et al., 1999). In these studies, a link was made between changed receptor expression in pyramidal cells and learning, although, at least in several models, the genetic modification affected interneurons as well. The present study examines the effect of reduced excitability in GABAergic interneurons at the network and behavioral level. We chose to reduce the excitatory drive in specific GABAergic interneurons, the PV-positive cells, by genetic modification of their AMPA receptors. Two mouse models with reduced excitatory drive on PV-positive interneurons were generated: the selective reduction of the AMPA-mediated current in PV-positive neurons was achieved either by the knockout of the GluR-D or of the GluR-A subunit in PV-positive GABAergic interneurons.

The choice of the two knockouts was based on previous studies that had shown differential expression of AMPA receptor subtypes in neurons of the hippocampus and cortex. In situ hybridization (Catania et al., 1995, 1998; Racca et al., 1996), immunocytochemistry (Kondo et al., 1997; Leranth et al., 1996; Petralia et al., 1997), and single-cell PCR studies (Angulo et al., 1997; Geiger et al., 1995; Jonas et al., 1994) revealed that at least in the hippocampus the preferential combination of AMPA receptor subunits is GluR-A plus GluR-B in pyramidal neurons and GluR-A plus GluR-D in interneurons. It was also shown that the differential expression pattern in pyramidal and GABAergic interneurons accounted for functional differences of AMPA receptors in the two cell populations (Geiger et al., 1995).

The two genetic manipulations selectively affected mainly PV-positive/FS cells, and the reduction of AMPA receptor-mediated current was comparable in *GluR-D*^{-/-} and in *GluR-A*^{PVCre-/-} mice. The functional role of this neuronal type for the generation and maintenance of synchronous gamma oscillations had been demonstrated in several studies (Gloveli et al., 2005; Joho et al., 1999; Sik et al., 1995). To directly show the effect of reduced PV-positive cell recruitment for hippocampal neuronal networks, we studied kainate-induced gamma oscillations in acute hippocampal slices from *GluR-D*^{-/-} and in *GluR-A*^{PVCre-/-} mice. Although AMPA receptor subunit expression in hippocampal pyramidal neurons remained unchanged, alterations in the population activity of pyramidal cells occurred, as indicated by reduction in power of

gamma oscillations in both models. Even though the genetic manipulations described here are discrete and affect only a subpopulation of GABAergic interneurons, their reduced recruitment is associated with impairments in specific hippocampus-dependent behavioral tasks in *GluR-D*^{-/-} and *GluR-A*^{PVCre-/-} mice. The observed deficits at the behavioral level were also similar in both models, indicating that sufficient excitation of PV-positive/FS interneurons is essential for several complex network activities.

RESULTS

Preferential Loss of GluR-D in PV-Positive Interneurons

GluR-D^{-/-} mice were generated using the Cre-lox system, and the removal of exon 11 led to the deletion of the first two transmembrane regions of the GluR-D subunit (Figure 1A, upper left panel). Successful targeting of the GluR-D locus and the subsequent establishment of the *GluR-D*^{-/-} mice was verified using Southern blot analysis (Figure 1A, upper right panel). The deletion of the subunit was verified by in situ hybridization and immunocytochemistry, which revealed the absence of the signal that is present in the wild-type (wt) (see Figure S1 in the Supplemental Data available online; Figure 1A, lower panels, left).

GluR-D expression has been previously demonstrated in identified FS cells in the hippocampus (Angulo et al., 1997; Geiger et al., 1995; Lambolez et al., 1996). FS cells are a major subclass of GABAergic interneurons, and they are known to express PV (Freund and Buzsaki, 1996; Kawaguchi et al., 1987; Kawaguchi and Kubota, 1997; Klausberger et al., 2002; Pawelzik et al., 2002). To assess the overall colocalization of GluR-D and PV in the hippocampus, double-labeling immunocytochemistry studies were carried out (Figure 1A, lower panels, right). The quantitative evaluation revealed that in fact the majority of GluR-D-positive cells in the hippocampus are PV positive. Thus, in CA1, 86.6% ± 9.15% and, in CA3, 82.3% ± 9% of GluR-D-positive neurons (slices from three animals) contain PV. To demonstrate that the FS cells analyzed in this study are indeed PV positive, biocytin-filled FS cells in the CA1 region were analyzed for PV expression (Figure S4). In *GluR-D*^{-/-} mice the pattern and number of PV-positive cells is not altered (data not shown), indicating that the development and survival of this cell population is not affected by the lack of the GluR-D subunit. GluR-D expression was also found in calbindin (CB)-positive cells in stratum radiatum, constituting thereby a minor population of GluR-D-expressing neurons. Somatostatin-positive oriens-lacunosum moleculare (OLM) cells do not express GluR-D.

Loss of GluR-A Expression in PV-Positive Interneurons

Since the GluR-A subunit is expressed in pyramidal neurons and GABAergic interneurons, a selective ablation in PV-positive cells required the generation of transgenic

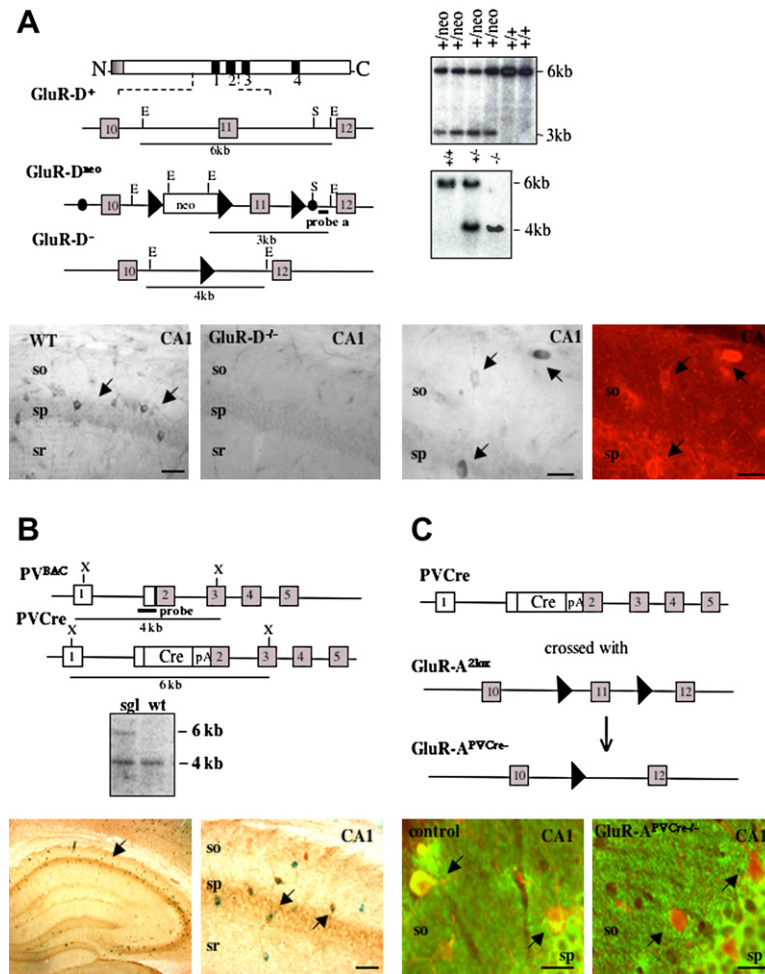


Figure 1. Generation of Two Transgenic Mouse Lines with Specific Ablation of AMPA Receptor Subunits

(A) Generation of *GluR-D*^{-/-} mice. Upper panel, left: Schematic representation of the *GluR-D*⁺ allele around exon 11, the targeted *GluR-D*^{neo} allele, and the *GluR-D*⁻ allele after Cre-mediated recombination. Black boxes represent membrane segments M1 to M4; open boxes are exonic sequences and the neo gene. LoxP sites are indicated by black triangles. Solid circles in *GluR-D*^{neo} indicate 5' and 3' ends of the targeting construct. Positions of EcoRV (E) and SacI (S) restriction sites are given. "Probe a" represents the fragment that was used as an outside probe for Southern blot analysis. Upper panel, right: Southern blot analysis of EcoRV-digested ES cell DNA showing the correct targeting of the *GluR-D*^{neo} vector. Southern blot analysis of mouse tail DNA from wt, heterozygous, and *GluR-D*^{-/-} mice after Cre-mediated excision. Lower panels, left: Distribution of the *GluR-D* subunit in the CA1 region of the hippocampus visualized by immunostaining in coronal sections of wt and *GluR-D*^{-/-} mice. The arrows indicate GABAergic interneurons expressing the *GluR-D* subunit in the wt hippocampus. Scale bars, 50 μ m. Lower panels, right: Double-immunostaining for *GluR-D* (left) and PV (right) in the CA1 of the hippocampus of wt mice. Arrows indicate double-positive cells. Scale bars, 50 μ m.

(B) Generation of transgenic animals with Cre recombinase expression in PV-positive neurons. Upper panel: Schematic representation of the PV gene structure and the modified PV gene located on a BAC. Southern blot analysis of tail DNA isolated from wt and transgenic mice digested with XbaI (X) to compare signal intensities of the wt and the single integrated copy of the transgene band. Lower panels: Cell type-specific recombination of the ROSA26 reporter. Higher magnification shows colabeling of PV (brown) with X-gal staining (blue) in the adult hippocampus. Scale bar, 50 μ m.

(C) Generation of the conditional *GluR-A*^{PVCre-/-} mice by crossing PVCre mice with *GluR-A*^{2lox} mice. Upper panel: Expression of Cre recombinase leads to Cre-mediated ablation of the *GluR-A* gene only in PV-positive cells. Lower panels: Double-labeling for PV (red) and *GluR-A* (green) expression in the CA1 region of control (left) and *GluR-A*^{PVCre-/-} (right) mice. Scale bar, 30 μ m. so, stratum oriens; sp, stratum pyramidale; sr, stratum radiatum.

mice that express Cre recombinase in this cell population. Hence, transgenic mice that express Cre recombinase under the control of the PV-promotor were generated. The bacterial artificial chromosome (BAC) technique (Meyer et al., 2002) was used, and out of two lines with detectable Cre recombinase expression in PV-positive interneurons (data not shown), one line was chosen for further analysis (Figure 1B).

To determine the pattern of PV-driven Cre-mediated recombination in transgenic mice, they were crossed with mice carrying the reporter R26R (Soriano, 1999). In the R26R strain, Cre-mediated recombination enables expression of *lacZ*-encoded β -galactosidase. The pattern of *lacZ* expression in adult PVCre; R26R corresponded to that described for PV-positive interneurons in the hippocampus (Celio, 1990; Kosaka et al., 1987), and indeed, we could detect PV immunoreactivity in the majority of *lacZ*-positive cells (Figure 1B). In cortex, Cre recombinase

activity was found only in a subpopulation of PV-positive cells and in a low number of PV-positive cells in other brain regions, such as amygdala and striatum (Figure S2).

The selective knockout of *GluR-A* in PV-positive interneurons was generated by breeding PVCre mice with *GluR-A*^{2lox} mice carrying a "floxed" exon 11 of the *GluR-A* subunit (Zamanillo et al., 1999). To demonstrate the selective ablation of *GluR-A*, double-labeling immunocytochemistry studies were carried out, and colocalization of *GluR-A* and PV in the adult hippocampus and other brain regions of control (homozygous *GluR-A*^{2lox} mice) and *GluR-A*^{PVCre-/-} mice was investigated (Figure 1C and Figure S2). Expression of *GluR-A* could be detected in PV-positive cells in the control but not in the hippocampus of adult *GluR-A*^{PVCre-/-} mice.

The effective loss of *GluR-A* expression is determined both by the transgene expression plus the expression of the endogenous "floxed" gene (here *GluR-A*) (Figure S3).

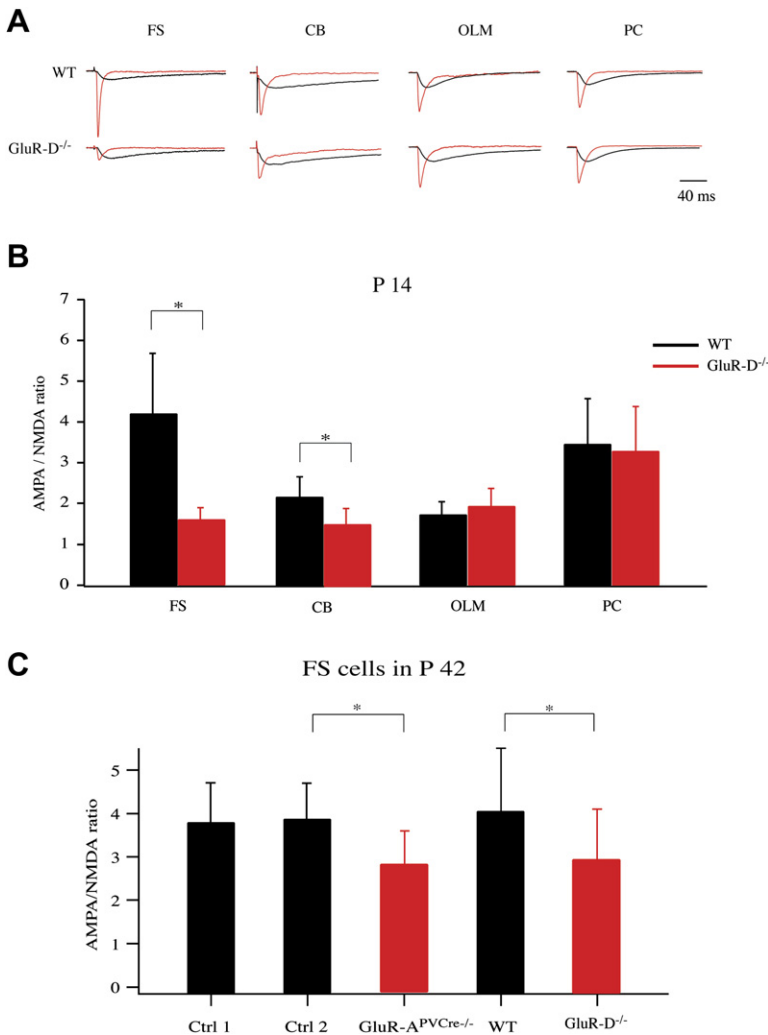


Figure 2. AMPA Receptor-Mediated Currents Are Reduced in *GluR-D*^{-/-} and *GluR-A*^{PVCre-/-}

(A) Synaptic AMPA (red) and NMDA (black) EPSCs were evoked by extracellular stimulation and were recorded from PV-positive fast-spiking (FS), calbindin-positive (CB), somatostatin-positive OLM, and pyramidal (PC) cells in slices from P14 wt and *GluR-D*^{-/-} animals. Traces are averages of 50–100 sweeps (scale bar 40 ms).

(B) Bar histogram represents average AMPA/NMDA ratios ± SD obtained for different hippocampal neuronal subtypes in slices from P14 wt (black bars) and *GluR-D*^{-/-} (red bars) mice.

(C) Bar histogram represents averaged values of AMPA/NMDA ratios ± SD obtained for PV-positive cells in slices from P42 *GluR-D*^{-/-} and *GluR-A*^{PVCre-/-} animals with their corresponding controls. Ctrl 1, *GluR-A*^{2lox} mice; Ctrl 2, PVCre mice.

Thus, this approach resulted in a preferential loss of *GluR-A* in PV-positive interneurons of the hippocampus but less in interneurons of other brain regions.

Reduction of AMPA Receptor-Mediated Currents in *GluR-D*^{-/-} and *GluR-A*^{PVCre-/-} Mice

The predominant expression of *GluR-D* in PV-positive cells permits the prediction that at a functional level the cell population that will be most significantly affected is comprised of FS cells. Indeed, electrophysiological studies carried out in FS, CB, and OLM cells of the hippocampal CA1 region revealed that the functional change preferentially affected FS cells (Figures 2A and 2B). Identification of the recorded GABAergic interneurons was based on the spiking pattern and confirmed by immunocytochemistry studies (Figure S4).

Evoked synaptic AMPA receptor-mediated currents in FS cells in P14 *GluR-D*^{-/-} mice were strongly reduced compared to those in wt controls as indicated by a much smaller AMPA/NMDA ratio that was 4.2 ± 1.5 in wt ($n = 12$ cells from 5 animals) and 1.6 ± 0.3 in *GluR-D*^{-/-}

mice ($n = 13$ cells from 4 animals; $p < 0.001$). In CB cells, reduction of the AMPA component was also seen, but to a lesser degree; AMPA/NMDA ratios were 2.19 ± 0.5 in the wt and 1.52 ± 0.39 in the *GluR-D*^{-/-} mice; $n = 8$ cells each from 3 and 4 animals, respectively; $p < 0.01$). In contrast, the relative amplitude of synaptic AMPA receptor-mediated currents in OLM cells remained unchanged. AMPA/NMDA ratios were 1.72 ± 0.32 and 1.93 ± 0.44 in wt and *GluR-D*^{-/-}, respectively ($n = 9$ from 2 animals each). Most importantly, the *GluR-D* deletion did not cause any reduction of AMPA currents in pyramidal cells where AMPA/NMDA ratios were 3.45 ± 1.12 in wt and 3.28 ± 1.1 in *GluR-D*^{-/-} ($n = 6$ cells from 2 animals each). Analysis of kinetic properties of spontaneous AMPA receptor-mediated currents in FS cells revealed that the rise time was not significantly different in wt and in *GluR-D*^{-/-} mice. However, the decay time in FS cells in *GluR-D*^{-/-} mice was slower (2.29 ± 0.73 ms in wt; 2.92 ± 0.9 ms in *GluR-D*^{-/-}; $n = 6$ cells for each; $p < 0.001$). This is consistent with previous studies showing that *GluR-D* expression in FS cells is an important

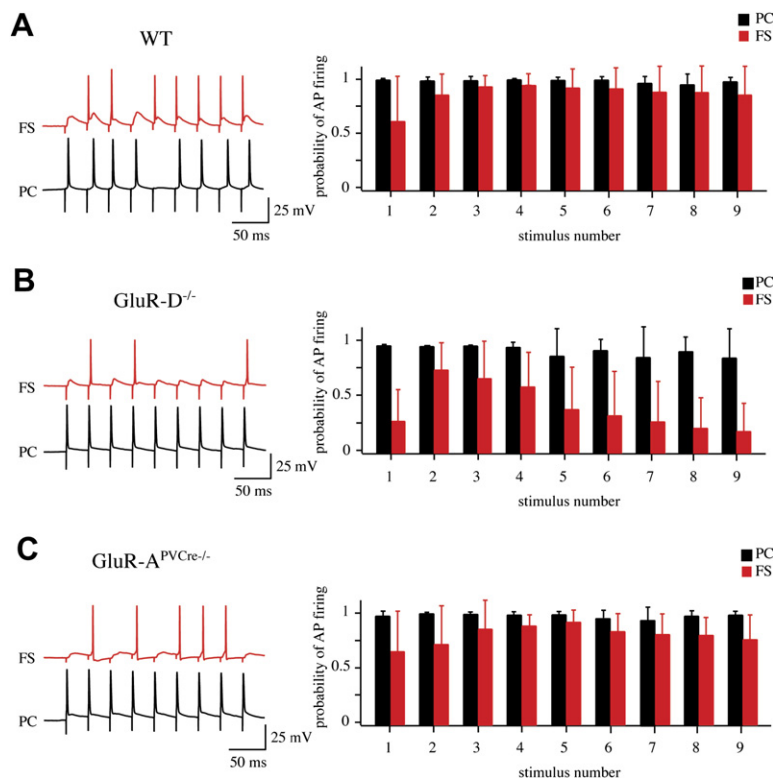


Figure 3. Reduction of FS Cell Output Due to Reduced CA3 to CA1 Excitatory Input

The probabilities of AP firing upon stimulation of CA3 pyramidal cell afferents were compared in (FS) and pyramidal cells (PC) in wt and mutant animals. Recordings were performed in the presence of bicuculline (5 μ M). Bar histograms on the right summarize average AP probabilities \pm SD in FS and PC cells in wt (A), *GluR-D^{-/-}* (B), and *GluR-A^{PvCre-/-}* animals (C). Example traces for each genotype are shown on the left (PV-positive interneuron in red and pyramidal cell in black).

determinant for the fast AMPA receptor deactivation in this cell population (Angulo et al., 1997; Geiger et al., 1995; Lambolez et al., 1996). In *GluR-D^{-/-}* mice, there was no change in kinetic properties of synaptic AMPA receptor-mediated currents in pyramidal cells as compared to controls (data not shown). Based on these studies of synaptic AMPA receptor-mediated currents in identified cells, one can conclude that the major effect of the GluR-D deletion will be an insufficient excitation of FS cells and hence reduced perisomatic inhibition that normally derives to a large extent from this cell population.

In *GluR-A^{PvCre-/-}* mice, a reduction of the AMPA current is expected to occur only at later developmental stages for two reasons. First, Cre recombinase is not expressed before the second postnatal week since it is under control of the parvalbumin promoter (Solbach and Celio, 1991; Soriano et al., 1992). Second, some time is required before Cre-mediated recombination occurs in both GluR-A alleles. Indeed, no reduction of the AMPA current was found in FS cells at P14 in *GluR-A^{PvCre-/-}* mice. A functional change, however, could be measured in the adult (P42). AMPA/NMDA ratio experiments revealed that the excitatory drive on PV-positive interneurons was significantly reduced in P42 *GluR-A^{PvCre-/-}* mice (Figure 2C). The appropriate "controls" for these experiments were FS cells from mice expressing either only the Cre recombinase (*PvCre* mice) or from mice with the "floxed" GluR-A alleles. In *GluR-A^{PvCre-/-}* mice, the AMPA/NMDA ratio was 2.8 ± 0.8 ($n = 10$ cells from 3 animals) compared to 3.9 ± 0.8 ($n = 7$ cells from 2 animals) in

GluR-A^{2lox} animals and 3.8 ± 0.9 ($n = 8$ cells from 4 animals) in *PvCre* animals (t test with Bonferroni correction, $p < 0.05$). To compare the reduction of AMPA-mediated currents in *GluR-A^{PvCre-/-}* mice with those in *GluR-D^{-/-}* mice, measurements were also carried out at P42 for *GluR-D^{-/-}* animals. The AMPA/NMDA ratio was 2.8 ± 1 ($n = 10$ from 6 animals) in *GluR-D^{-/-}* compared to 4.1 ± 1.4 ($n = 10$ cells from 3 animals) in wt littermates ($p < 0.05$). Thus, a comparable reduction of the excitatory input onto PV-positive interneurons could be demonstrated at P42 in *GluR-D^{-/-}* and *GluR-A^{PvCre-/-}* mice. The decay time of evoked EPSCs in FS cells was slower in *GluR-D^{-/-}* but was not changed in *GluR-A^{PvCre-/-}* mice compared to controls (data not shown).

To assess the effect of reduced excitation on FS cells in the mutants, their output was studied and compared to controls (Figure 3). Firing activity of CA1 FS and pyramidal cells were evoked by rhythmic extracellular stimulation (nine pulses at 20 Hz) in the CA3 region in *GluR-D^{-/-}*, *GluR-A^{PvCre-/-}*, and wt mice. Whole-cell current-clamp recordings were performed simultaneously from an FS cell and an adjacent CA1 pyramidal cell at P42. In both mutants, stronger stimuli were required to induce AP firing in FS cells. To compare between mutants and control animals, a stimulus pulse of 10 mA in amplitude and 500 μ s in duration was chosen. This regime led to AP firing with an average probability close to 1 in FS and pyramidal cell in wt. Compared to wt, where the average probability of AP firing in FS cells was 0.87 ± 0.22 ($n = 8$ cells from 6 animals), the average probability of AP firing in *GluR-D^{-/-}*

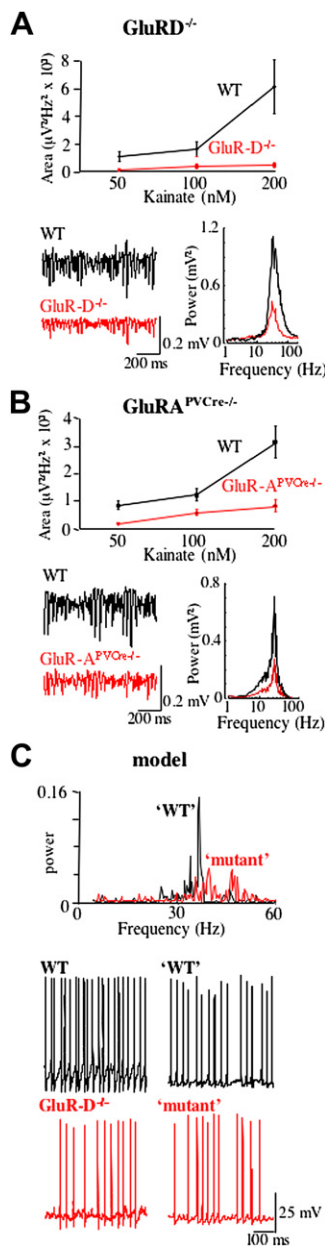


Figure 4. Disrupted Field Gamma Oscillations Accompany Reduced Interneuron Recruitment

(A) Power of gamma oscillations in area CA3 was reduced in slices from *GluR-D*^{-/-} mice compared to wt mice. Graph shows mean area power \pm SEM (20–80 Hz) for slices from wt (n = 8, black) and *GluR-D*^{-/-} mice (n = 9, red). Example traces show 1 s of stratum radiatum field gamma oscillations in the presence of 200 nM kainate. Scale bars, 200 ms, 0.2 mV. Graph shows pooled power spectra (n = 5, 60 s data epochs) for gamma rhythms induced by 200 nM kainate in slices from control (black) and *GluRD*^{-/-} (red) mice.

(B) The power of gamma oscillations recorded in stratum radiatum of area CA3 was also reduced in slices from *GluRA*^{PVCre-/-} mice compared to wt. Graph shows mean area power \pm SEM (20–80 Hz) for slices from wt (n = 5, black) and *GluA*^{PVCre-/-} mice (n = 7, red). Example traces show 1 s of stratum radiatum field gamma oscillations in the presence of 200 nM kainate. Scale bars, 200 ms, 0.2 mV. Graph shows

was reduced to 0.41 ± 0.33 (n = 8 cells from 6 animals) and somewhat less in *GluR-A*^{PVCre-/-} mice, where the average probability of AP firing was 0.78 ± 0.23 (n = 13 from 5 animals cells; $p < 0.001$, Kruskal-Wallis one-way analysis of variance on ranks; $p < 0.05$, Dunn's Method for pairwise comparison of wt versus *GluR-D*^{-/-}, wt versus *GluR-A*^{PVCre-/-}, and *GluR-D*^{-/-} versus *GluR-A*^{PVCre-/-}). There was no difference between the probability of AP firing in pyramidal cells in mutants and controls (0.95 ± 0.12 for *GluR-D*^{-/-}, n = 8 from 6 animals; 0.94 ± 0.1 for *GluR-A*^{PVCre-/-}, n = 13 from 5 animals; 0.98 ± 0.04 for wt, n = 8 from 6 animals; $p = 0.202$, Kruskal-Wallis one-way analysis of variance on ranks).

Reduced Excitation of Fast-Spiking Interneurons Disrupts Hippocampal Gamma Rhythms In Vitro

Gamma oscillations originate in area CA3 and project to area CA1 in vivo (Csicsvari et al., 2003) and in vitro (Fisahn et al., 1998). The principal interneuron subtype involved in gamma rhythm generation is perisomatic targeting FS cells, which receive large, rhythmic excitatory postsynaptic potentials from CA3 pyramidal cells during the oscillations (Gloveli et al., 2005; Mann et al., 2005). Given the largely selective deficits in CA3 pyramidal cell inputs to perisomatic targeting FS cells (see above), we examined the consequences of *GluR-D* and *GluR-A* ablation in FS/PV-positive cells for gamma rhythms. To assess whether the changes we observed were directly attributable to the genetic manipulation, we also compared experimental data to a network model of gamma rhythms in which only the profile of EPSCs to interneurons was altered.

Persistent field potential gamma oscillations were generated in acute hippocampal slices by bath application of kainate (50–200 nM), a concentration range that produces gamma frequency field potential amplitudes ranging from the small amplitudes seen in persistent rhythms in vivo to the larger amplitudes (up to 1 mV) seen following physiological sharp waves in awake behaving rodents (Traub et al., 1996). At each concentration of kainate used, the power of gamma oscillations in both area CA3 and CA1 was significantly larger in slices from wt mice than in slices from *GluR-D*^{-/-} or *GluR-A*^{PVCre-/-} mice (Figures 4A and 4B). Maximal integral area power (20–80 Hz) for wt was

pooled power spectra (n = 5, 60 s data epochs) for gamma rhythms induced by 200 nM kainate in slices from control (black) and *GluRA*^{PVCre-/-} (red) mice.

(C) Model data predict the disrupted gamma power and implicate reduced interneuron recruitment. Graph shows single spectra from model field potentials (inverted average of somatic membrane potential changes) for control (black) conditions and conditions where phasic input to interneurons was modified according to the biophysical data collected from slices from *GluRD*^{-/-} mice. Example traces (left panel) are taken from stratum pyramidale FS interneurons from slices from wt (black) and *GluRD*^{-/-} (red) mice. Note the increased incidence in gamma periods with no interneuron output in *GluRD*^{-/-} (red) condition. Example traces (right panel) show corresponding model interneuron data revealing reduced interneuron action potential generation per underlying gamma period. Scale bars, 100 ms, 25 mV.

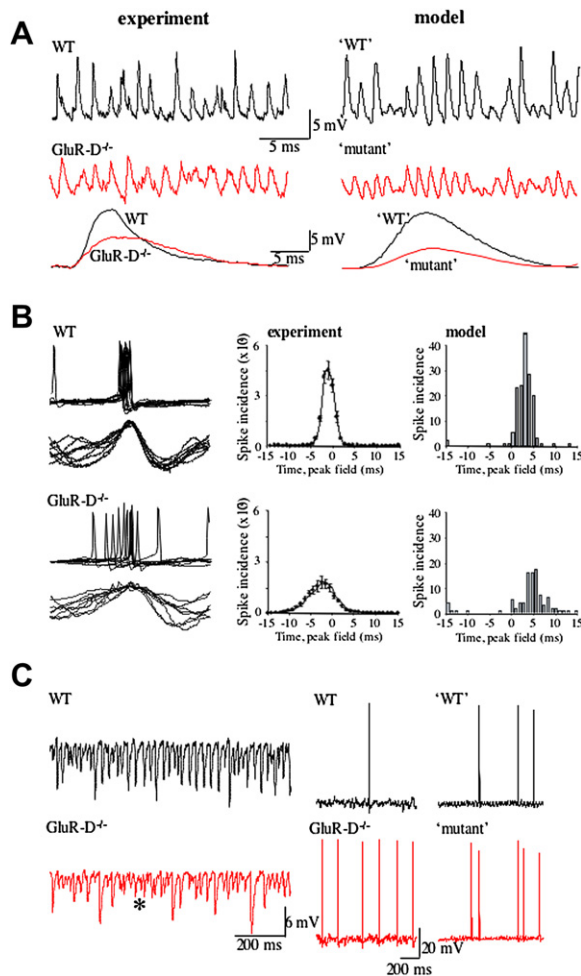


Figure 5. Disrupted AMPA Receptor Inputs to Interneurons Leads to Imprecision in Action Potential Outputs and Consequently a Reduced Gamma Frequency Inhibitory Drive to Principal Cells

(A) At a membrane potential of -70 mV, EPSPs in interneurons during gamma oscillations were smaller and broader in slices from *GluR-D^{-/-}* compared to wt mice. Lower traces show mean EPSPs ($n = 10$) from wt and *GluR-D^{-/-}* mice on expanded time scale (see text for more detailed statistical analysis). Equivalent data from the model are shown on the left, where, again, only changing the synaptic activation parameters to interneurons reproduced the observed changes in compound, phasic excitatory input during network behavior.

(B) Modified AMPA inputs were accompanied by disrupted precision of spike timing in CA3 interneurons in slices from *GluR-D^{-/-}* mice compared with wt. Traces show ten overlaid periods of gamma oscillation (40 ms window) aligned to the peak positivity of the concurrently recorded field potential in CA3 stratum radiatum. Graphs show histograms of spike incidence (1 ms bin width) with respect to field potential (0 ms = peak field positivity) averaged for 2 min of continuous gamma oscillation in four interneurons from four different animals in each case. Model histograms were from 3500 s of data with spike times referenced to the somatic “field” minimum. In both experiment and model, interneuron spikes were more broadly temporally distributed.

(C) The reduced and temporally more imprecise output from interneurons generates smaller, more erratic trains of IPSPs in principal cells. Example traces (left panel) show 1 s of data recorded from pyramidal cell somata at -30 mV in slices from wt (black) and *GluR-D^{-/-}* mice.

$6150 \pm 1940 \mu\text{V}^2 \cdot \text{Hz}$ ($n = 8$ slices, each from a different animal) and in slices from *GluR-D^{-/-}* mice $457 \pm 174 \mu\text{V}^2 \cdot \text{Hz}$ ($n = 9$; $p < 0.05$). In experiments using *GluR-A^{PVCre-/-}* mice, peak power (20–80 Hz) for wt was $3041 \pm 570 \mu\text{V}^2 \cdot \text{Hz}$ ($n = 5$ slices, each from a different animal) and in slices from *GluR-A^{PVCre-/-}* mice $733 \pm 214 \mu\text{V}^2 \cdot \text{Hz}$ ($n = 5$; $p < 0.05$). Changing the phasic interneuron drive in the model to match the observed changes in compound EPSP/C inputs to interneurons (see Figure 5) also produced a dramatic decrease in gamma power (Figure 4C). Median peak frequency of gamma oscillations was not significantly different at concentrations of kainate above 50 nM ($p > 0.05$), but a small, significant decrease in peak frequency was seen at the 50 nM level (wt 35 [32–36] Hz versus *GluR-D^{-/-}* 33 [28–34] Hz; $p < 0.05$).

The model predicted that the decrease in gamma field power was caused by a change in interneuron recruitment patterns (Figure 4C). Changing only the profile of unitary excitatory synaptic input to interneurons reduced interneuron spiking from, on average, 0.84 spikes per period of gamma oscillation in wt simulations to 0.46 spikes per period in mutant simulations. We tested this prediction by examining spike activity in fast-spiking CA3 interneurons, with cell bodies in stratum pyramidale. Interneuron spiking was markedly changed in *GluR-D^{-/-}* mice compared with wt. Action potential incidence was significantly reduced from 0.92 ± 0.05 spikes per gamma period in interneurons of wt mice, to 0.66 ± 0.13 spikes per gamma period in interneurons from *GluR-D^{-/-}* mice (1000 periods from $n = 4$ cells from 4 animals in each group, $p < 0.05$; Figure 4C).

Spiking in interneurons during persistent gamma oscillations is predominantly mediated by strong, phasic synaptic excitation. The profile of unitary synaptic excitatory events in interneurons was specifically disrupted in the genetic models used here (see above). To test whether this change was manifest in phasic synaptic drive during gamma rhythms, we examined EPSP profiles during the population rhythm. Compound EPSPs in interneurons, recorded at -70 mV, were significantly smaller in slices from *GluR-D^{-/-}* mice (wt 12.2 ± 0.8 mV versus *GluR-D^{-/-}* 7.8 ± 1.0 mV; 1000 periods each from $n = 4$ interneurons from 4 animals in each group, $p < 0.05$). The smaller EPSPs in slices from *GluR-D^{-/-}* mice also had longer decay times (wt 4.8 ± 0.8 ms versus *GluR-D^{-/-}* 7.5 ± 1.2 ms; $p < 0.05$; Figure 5A), indicating that the changes in AMPA receptor subunit composition in specific interneurons was functionally manifest during network gamma rhythms.

Asterisk denotes example of a prolonged period of irregular, small IPSPs. See main text for statistical analysis of IPSP changes. Scale bars, 100 ms, 6 mV. Example traces in the right panel show the greater incidence of pyramidal cell somatic action potential generation during gamma oscillations. Traces show 1 s of data from somatic intracellular recordings from wt (black) and *GluR-D^{-/-}* (red) mice. An increase in pyramidal cell recruitment was also seen in the model (compare “wt” and “mutant”). Scale bars, 200 ms, 20 mV.

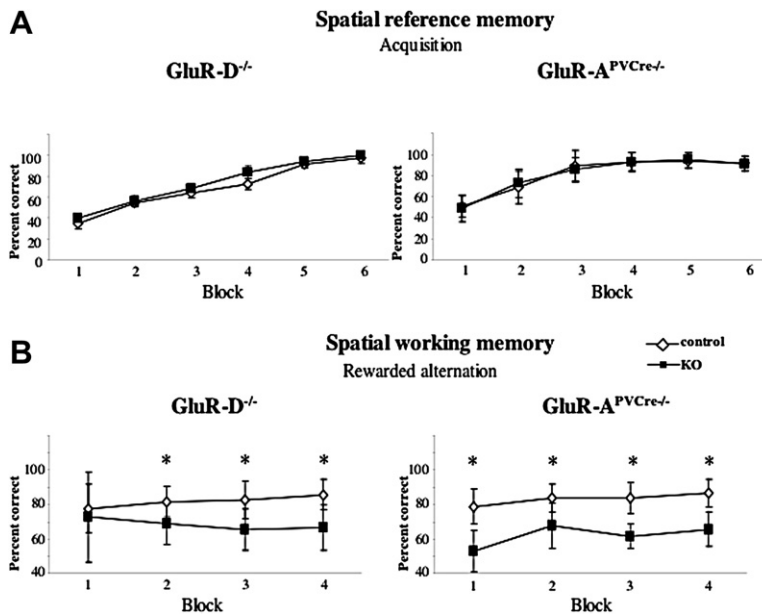


Figure 6. Unaltered Spatial Reference Memory but Impaired Spatial Working Memory in *GluR-D*^{-/-} (Left Panel) and *GluR-A*^{PVCre-/-} (Right Panel) Mice

(A) Mean percent correct responses (\pm SEM) during acquisition of an appetitive hippocampus-dependent spatial reference memory task on the elevated Y maze for control (white diamonds) and *GluR-D*^{-/-} or *GluR-A*^{PVCre-/-} mice (black squares) (wt n = 9, *GluR-D*^{-/-} n = 13; control n = 9, *GluR-A*^{PVCre-/-} n = 8). (B) Mean percent correct responses (\pm SEM) during hippocampus-dependent spatial non-matching-to-place testing on the elevated T maze ($p < 0.01$ for all four blocks) (wt n = 16, *GluR-D*^{-/-} n = 16; control n = 18, *GluR-A*^{PVCre-/-} n = 12). Note that the *GluR-D*^{-/-} mice did not differ significantly from the wt animals for the first block of ten trials. Each block represents a score out of ten trials for both the Y maze and the elevated T maze.

Along with the overall reduction in interneuronal spike generation associated with the changes in phasic excitatory drive to interneurons, there was also some evidence for a disruption in temporal precision of spikes. There was an increase in the variability of action potential timing with respect to the local field potential oscillation (Figure 5B). It should be noted that the amplitude of the field potential rhythm was reduced in mice with disrupted AMPA receptor inputs to FS interneurons. This would be expected to reduce the temporal precision of the measurements taken (i.e., the relationship between interneuron spike precision and field potential amplitude may be causal or effectual). However, a broader distribution of interneuron spikes with respect to the population rhythm was also seen in model simulations where signal/noise ratio was not an issue.

Accompanying this change in interneuron output patterns was a change in population IPSP expression in CA3 pyramidal cells during gamma oscillations. There was a decrease in the incidence of large, compound IPSPs and an increase in bursts of smaller IPSPs during any given gamma period (Figure 5C). This resulted in a significant decrease in overall IPSP amplitude at -30 mV membrane potential during gamma rhythms in pyramidal cells in mice with modified interneuronal AMPA receptor subunit composition (7.4 ± 0.8 mV, 1000 IPSPs each from n = 6 pyramidal cells from 6 wt animals versus 5.1 ± 0.7 mV, 1000 IPSPs each from n = 6 pyramidal cells from 6 *GluR-D*^{-/-} animals; $p < 0.05$). This change in phasic inhibitory input to pyramidal cells during the gamma rhythm was accompanied by altered action potential output characteristics. Interspike intervals in pyramidal cells during gamma oscillations decreased from 0.92 ± 0.01 s (1000 periods from n = 5 cells from 5 animals) in wt to 0.18 ± 0.12 s (1000 periods from n = 5 cells from 5 animals) in slices from *GluR-D*^{-/-} mice ($p < 0.005$; Figure 4C). CA3

pyramidal cells also had a more depolarized mean membrane potential during gamma oscillations (wt -62 ± 2 mV versus *GluR-D*^{-/-} -56 ± 4 mV; n = 6 animals; $p < 0.05$) and an increase in input resistance from 34 ± 2 M Ω (wt) to 50 ± 3 M Ω (*GluR-D*^{-/-}, n = 6 animals; $p < 0.005$). However, this increase in intrinsic excitability was not accompanied by an increase in EPSP amplitudes in CA3 pyramidal cells. Mean EPSP amplitudes were 2.1 ± 0.2 mV (wt) and 2.4 ± 0.2 mV (*GluR-D*^{-/-}) at -70 mV membrane potential ($p > 0.3$ data not shown), suggesting it was a consequence of disrupted inhibitory drive.

Reduced Excitation of Fast-Spiking Interneurons Affects Hippocampus-Dependent Working Memory and Disrupts Short-Term Recognition Memory

Given the altered pattern of hippocampal interneuronal activation on one hand and the well-documented involvement of the hippocampus in spatial learning and memory on the other, we performed behavioral studies whose major focus were tasks that are sensitive to hippocampal dysfunction.

Since the *GluR-D* gene was deleted throughout the brain, a test battery assessing sensorimotor, affective, and cognitive behavior was used to analyze the behavioral phenotype of the *GluR-D*^{-/-} mice. Anxiety and spontaneous locomotor activity was not affected in *GluR-D*^{-/-} mice (Figure S5). In *GluR-D*^{-/-} mice, spatial reference memory was assessed using two tests, an appetitive spatial reference memory task on an elevated Y maze and the standard, fixed-location, hidden-platform version of the Morris water maze (Morris et al., 1982; Reisel et al., 2002). On both tasks, *GluR-D*^{-/-} and wt animals learned equivalent rates and reached the same levels of performance (Figure 6A and Figure S6). The *GluR-A*^{PVCre-/-} mice also showed unimpaired spatial reference memory. There was no difference between *GluR-A*^{PVCre-/-} and control

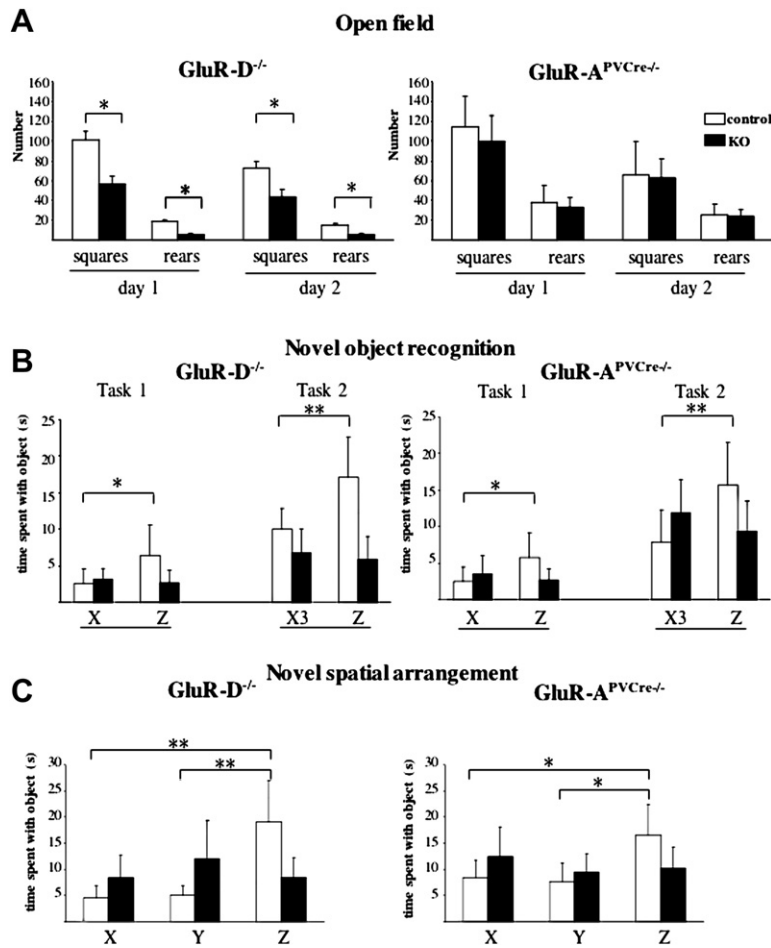


Figure 7. Differences during Exploratory Behavior and Impaired Novel Object Recognition and Spatial Rearrangement-Induced Exploration in *GluR-D^{-/-}* and *GluR-A^{PVCre-/-}* Mice

(A) *GluR-D^{-/-}* mice crossed fewer squares and reared significantly less than control animals in a dark gray painted version of an open field test using normal room illumination ($p < 0.01$); *GluR-A^{PVCre-/-}* mice showed no alterations compared to the control animals. The test was performed twice on two consecutive days. (wt $n = 9$, *GluR-D^{-/-}* $n = 13$; control $n = 18$, *GluR-A^{PVCre-/-}* $n = 11$).

(B) The novel object recognition test was performed 5 min after a 5 min sample phase. There were two separate protocols used. Task 1: In the sample phase of this test, the animal is allowed to explore two different objects (X and Y). The bars show the time the animal spent during the test phase exploring a new object (Z) and a duplicate of object X. Only control mice showed a clear preference for the novel object ($p < 0.02$). (wt $n = 16$, *GluR-D^{-/-}* $n = 16$; control $n = 18$, *GluR-A^{PVCre-/-}* $n = 11$). Task 2: Animals were allowed to explore two copies of an identical object (X1 and X2) during the sample phase. The bars show the time the animals spent during the test phase exploring a new object (Z) and a triplicate of object (X). Only control mice showed a clear preference for the novel object ($p < 0.001$) (wt $n = 11$, *GluR-D^{-/-}* $n = 11$; control $n = 17$, *GluR-A^{PVCre-/-}* $n = 12$). Between task 1 and task 2, animals performed the rewarded alternation on the T maze. Note, the effect on the overall increase in exploratory activity for all genotypes in task 2.

(C) Novel spatial arrangement task: Mice were presented with three different objects (X, Y, and Z) during two sample phases. Bars show the time spent with the triplicates of the three objects during the test phase, after the location of one of them (object Z) had been moved. Only control mice showed a preference for the displaced object Z ($p < 0.001$ for *GluR-D^{-/-}* controls, $p < 0.01$ for *GluR-A^{PVCre-/-}* controls) (wt $n = 14$, *GluR-D^{-/-}* $n = 11$; control $n = 17$, *GluR-A^{PVCre-/-}* $n = 11$). Each column represents the mean \pm SEM.

mice when tested in the appetitive spatial reference memory task on an elevated Y maze (Figure 6A). The performance of *GluR-A^{PVCre-/-}* mice was not analyzed with the standard version of the Morris water maze since it is well documented that even the complete *GluR-A* knockout showed no abnormality in this test (Reisel et al., 2002; Zamanillo et al., 1999).

Spatial working memory was assessed using hippocampus-dependent rewarded alternation (non-matching-to-place) on the T maze (Rawlins and Olton, 1982). *GluR-D^{-/-}* and *GluR-A^{PVCre-/-}* mice showed a moderate impairment of spatial working memory compared to control animals on this rewarded alternation task. The *GluR-D^{-/-}* mice did not differ significantly from the wt animals for the first block of ten trials (percent correct, wt $78.13\% \pm 13.6\%$; *GluR-D^{-/-}* $72.5\% \pm 13.6\%$; $p > 0.2$). However, the mutant mice showed a moderate impairment of correct responses during the next three blocks (overall mean for all blocks: percent correct, wt $83.5\% \pm$

13.9% ; *GluR-D^{-/-}* $67.3\% \pm 13.9\%$; $p < 0.01$) (Figure 6B). *GluR-A^{PVCre-/-}* mice expressed also a moderate impairment of correct responses (overall mean for all blocks: percent correct, control $83.6\% \pm 2.4\%$; *GluR-A^{PVCre-/-}* $62.3\% \pm 4.8\%$; $p < 0.01$) (Figure 6B).

Compared to wt mice, the *GluR-D^{-/-}* mice demonstrated reduced exploratory activity in response to novel environmental stimuli. During testing in the open field, the *GluR-D^{-/-}* mice made significantly fewer square crosses (number of squares, wt 101.6 ± 8.15 ; *GluR-D^{-/-}* 56.7 ± 6.78 ; $p < 0.01$) and reared significantly less on both days of testing (number of rears, wt 18.56 ± 2.14 ; *GluR-D^{-/-}* 5.08 ± 1.78 ; $p < 0.01$; Figure 7A). There was no difference in exploratory activity between control and *GluR-A^{PVCre-/-}* mice.

We also performed tests for object recognition and spatial change in the *GluR-D^{-/-}* and *GluR-A^{PVCre-/-}* mice. The measurement of rodents' ability to recognize novel objects (Alarcon et al., 2004; Rampon et al., 2000) and

spatial relationships among objects (DeCoteau and Kesner, 1998; Gilbert and Kesner, 2004; Mumby et al., 2002) is based on their natural exploratory behavior and their ability to remember previously encountered objects. Two different training protocols were used for object memory. The mice were exposed to two different objects (task 1) or to two identical objects (task 2) for 5 min during the training or sample session (Figure 7B). During training for task 1, there was no significant difference between groups in the total time spent exploring objects (time spent with objects X and Y, wt 9.9 ± 6.7 s; *GluR-D*^{-/-} 10.2 ± 6.3 s; $p = 0.94$; control 12.1 ± 5.4 s; *GluR-A*^{PVCre-/-} 8.6 ± 4.3 s; $p = 0.17$). But both wt and *GluR-D*^{-/-} mice showed significantly higher exploratory activity during the training session of task 2 (performed after the mice had finished the test for rewarded alternation on the T maze; time spent with objects X1 and X2, wt 27.1 ± 7.4 s; *GluR-D*^{-/-} 12.6 ± 6.5 s; $p < 0.001$). The increase in exploratory activity in task 2 was similar between the control and *GluR-A*^{PVCre-/-} mice (control 25.6 ± 12 s; *GluR-A*^{PVCre-/-} 20.3 ± 7.1 s; $p = 0.24$). Object recognition was assessed 5 min after the sample phase by expressing the time spent exploring the novel object compared to the time spent exploring the familiar object during the test phase. Wild-type mice spent more time exploring the novel objects, whereas *GluR-D*^{-/-} and *GluR-A*^{PVCre-/-} mice showed no such preference, regardless of training protocol during the sample phase.

The reaction to spatial change was assessed during a spatial recognition task (Figure 7C). There was no significant difference between the two groups in the total time spent exploring the three objects during the two training or sample sessions. For this test, three duplicates for each object were used. Wild-type mice recognized the spatial change in the arrangement of the objects by interacting more with the displaced object, whereas *GluR-D*^{-/-} and *GluR-A*^{PVCre-/-} mice did not exhibit such a preference (time spent with displaced object C, wt 19.1 ± 7.5 s; *GluR-D*^{-/-} 8.5 ± 3.7 s; control 16.6 ± 5.9 s; *GluR-A*^{PVCre-/-} 10.2 ± 4 s) and explored all three objects equally.

DISCUSSION

In this study, we made three principal observations concerning cellular/network physiology and behavior in *GluR-D*^{-/-} and *GluR-A*^{PVCre-/-} mice as compared with control mice. First, a pattern of disruption in pyramidal cell-mediated synaptic drive to predominantly PV-positive, perisomatic targeting interneurons was observed that resulted in a reduced output of this cell population. Second, persistent gamma oscillations in CA3 had reduced power in *GluR-D*^{-/-} and *GluR-A*^{PVCre-/-} mice. Finally, there were abnormalities in spatial working memory, novel object exploration, and the response to changes in the spatial relationships among multiple objects in *GluR-D*^{-/-} and *GluR-A*^{PVCre-/-} mice. The intact spatial reference memory we observed in the mutant mice rules

out a general sensorimotor or motivational explanation for these abnormalities. The two different genetic modifications are associated with a similar phenotype at the network and behavioral level, and thus an indirect, secondary mechanism is unlikely to be the basis of the observed deficits.

In two mouse models that were manipulated genetically in different ways—one a global knockout, the other a cell type-specific ablation—the cell type that was preferentially affected was the FS/parvalbumin-positive cells. The first approach, the knockout of the GluR-D subunit, affected mainly PV-positive cells. In fact our double-labeling immunocytochemistry corroborated that the majority of GluR-D-expressing cells in wt animals are PV-positive. The second approach, the selective GluR-A ablation, was based on the selectivity of Cre expression controlled by the parvalbumin promoter. The preferential ablation of GluR-D or GluR-A in FS PV-positive cells is most likely the reason why seizures were not observed in these mutant mice, neither in the slice nor in vivo during the extensive behavioral tests.

Deletion of the GluR-D or GluR-A subunit led to a strong reduction of AMPA receptor-mediated currents in PV-positive interneurons as evidenced by the reduction in the AMPA/NMDA ratios in P42 old animals. The consequence of the genetic manipulations was a change in the output of FS/PV-positive cells consisting in a reduced firing rate. Although at P42 the functional change of the AMPA receptor-mediated current is comparable in the two mutants, there is a difference in the onset of the current reduction. This difference can be accounted for by the promoter activity of the GluR-D and parvalbumin gene, respectively. The reduction of the AMPA current at P14 in *GluR-D*^{-/-} animals can be attributed to the early expression of the GluR-D subunit (Monyer et al., 1991). In contrast, Cre recombinase expression is controlled by the parvalbumin promoter, and the onset of the transgene does not occur before the second postnatal week. The difference in the temporal profile of the GluR-D and GluR-A ablation indicates that the similar phenotype cannot be accounted for by nonspecific or secondary mechanisms but is due to the reduced excitation of FS/PV-positive cells.

Previous studies showed that GluR-D and GluR-A are the major AMPA receptor subunits in FS/PV-positive cells, with only low expression levels of the other two subunits. These latter account for the residual AMPA receptor current in both mutants. There was, however, a difference between *GluR-D*^{-/-} and *GluR-A*^{PVCre-/-} mice in terms of kinetic properties of AMPA receptors in FS cells; the GluR-D knockout not only reduced amplitude but also slowed kinetics. In contrast, in *GluR-A*^{PVCre-/-} mice, the amplitude but not the kinetics was changed. This differential effect reflects distinctions in kinetic properties of the GluR-D and GluR-A subunit, as demonstrated for recombinant receptors (Burnashev et al., 1992).

Removal of the GluR-D or the GluR-A subunit generated a change in the pattern of synaptic excitation measured in

individual hippocampal interneurons. This change had consequences for network activity, as observed during population gamma rhythms. *GluR-D*^{-/-} mice have smaller (and slightly slower) interneuronal EPSCs. It is therefore not surprising that interneuron spike timing should be less precise and overall interneuronal firing reduced. Our network model is consistent with this notion, as reduction in amplitude and slight slowing of interneuron EPSC kinetics are sufficient to reproduce the cardinal experimentally observed alterations in gamma oscillation properties. The similar phenotype of the two mutants points to the amplitude as the critical variable underlying the observed abnormalities. We wish to point out that the *in vitro* pharmacological gamma protocol was chosen rationally, since pharmacological gamma has a number of cellular characteristics shared with *in vivo* hippocampal gamma oscillations which occur during exploration: in both sorts of oscillation, pyramidal neurons fire on a small proportion of the gamma waves, interneurons fire on a much larger proportion of the waves, and the phase of pyramidal cell firing slightly leads that of interneuron firing; in addition, both sorts of oscillation are modulated at theta frequency (Bragin et al., 1995; Csicsvari et al., 2003; Fisahn et al., 1998). PV-positive cells that preferentially target the perisomatic regions of principal cells participate in pharmacologically induced gamma oscillations *in vitro* (Gloveli et al., 2005; Mann et al., 2005) and also in hippocampal *in vivo* gamma oscillations (Sik et al., 1995); and both mouse lines affect preferentially PV-positive interneurons.

GluR-D and GluR-A ablation in PV-positive interneurons results in a reduced excitatory drive onto this subpopulation of GABAergic interneurons and hence to their inefficient recruitment. This manipulation translates into several hippocampus-related behavioral impairments with a similar phenotype of the two mutants. Similar changes were observed with respect to current reduction, gamma oscillations, and hippocampus-dependent behavior in *GluR-D*^{-/-} and *GluR-A*^{PVCre-/-} mice. One difference between the two mutants regarded their exploratory behavior that is reduced in the *GluR-D*^{-/-} but not in the *GluR-A*^{PVCre-/-} mice. The reduced exploratory activity in the *GluR-D*^{-/-} mice could reflect functional changes in additional interneurons other than PV/FS cells and/or the involvement of other brain regions in addition to the hippocampus. Indeed, cellular measurements showed that the ablation of the GluR-D subunit affected also a population of CB-positive interneurons. Indications that in the *GluR-D*^{-/-} mice PV/FS cells in other brain regions may be involved are based on the GluR-D expression *in wt*. Thus, GluR-D expression was found in the reticular thalamus and medial septum, but no GluR-A expression was detectable in these brain areas. Taken together, the differential regional expression of GluR-A and the restricted expression of Cre recombinase in the PVCre line used here guaranteed a higher specificity of the genetic manipulation that affected PV-positive cells mainly in hippocampus and cortex in *GluR-A*^{PVCre-/-} mice. Although in this study we focused on hippocampus-dependent behavior, we

cannot exclude the possibility that ablation of GluR-D or GluR-A in PV-positive cells in other brain areas other than the hippocampus (e.g., forebrain) influenced the behavioral deficits.

Although spatial reference memory acquisition in multi-trial tasks is normal in *GluR-D*^{-/-} and *GluR-A*^{PVCre-/-} mice, spatial working memory (Olton et al., 1979) as assessed by rewarded alternation (non-matching-to-place) on the T maze (Rawlins and Olton, 1982) is moderately impaired. Complete GluR-A knockout mice also exhibit normal spatial reference memory, and the deficit in spatial working memory is more pronounced than in the mutants described here (Reisel et al., 2002; Zamanillo et al., 1999). This is not surprising, considering that in those mice principal cells and interneurons must be affected. Indeed, the alteration of spatial working memory in *GluR-D*^{-/-} and *GluR-A*^{PVCre-/-} mice is striking considering that only about 20% of GABAergic interneurons have been genetically modified.

There is growing evidence that the hippocampus may act as a novelty detector identifying mismatches between incoming and stored information which has been thought to underlie exploratory behavior (Gray, 1982; Honey et al., 1998; Li et al., 2003; Vinogradova and Brazhnik, 1977). Exploratory behavior in rodents is accompanied by specific hippocampal EEG activity recorded *in vivo* (Buzsaki, 2002; O'Keefe and Nadel, 1978). This EEG activity takes the form of a large field theta rhythm upon which is superimposed a gamma rhythm (Chrobak and Buzsaki, 1998).

Deficits in exploratory behavior in *GluR-D*^{-/-} and *GluR-A*^{PVCre-/-} mice were revealed during the performance of the novel object recognition test as well as in a test based on the assessment of special relationships between objects. Recognition memory requires the discrimination between the novelty and familiarity of previous experiences. The selective spatial working memory impairment as well as the altered exploratory behavior in response to novel objects or the spatial arrangement of objects are consistent with the possibility that gamma activity in hippocampus and surrounding cortical areas may contribute to a flexible, episodic-like memory system (Fortin et al., 2002; Morris et al., 2003; Nakazawa et al., 2002; Reisel et al., 2002). Indeed, gamma activity in the human rhinal-hippocampal region has been associated with successful storage of information in declarative memory (Fell et al., 2001).

Oscillatory activities in the gamma range have not only been implicated in feature binding, but have also been detected during short-term memory maintenance when sustained activation of neural representations is required (Pezaran et al., 2002; Tallon-Baudry et al., 2001). During EEG recordings or intracranial recordings in humans (Howard et al., 2003), significant increases in gamma power are observed. Our data provide strong correlative evidence that reduced power of hippocampal gamma oscillations is associated with specific hippocampal memory deficits. Future *in vivo* recordings in the behaving animal will allow us to better correlate changes of gamma oscillations but

possibly also of other oscillatory activities that were not tested in this study with the impairments in the learning paradigms described here.

The data demonstrate that disruption of FS/PV-positive interneuron recruitment had consequences for pyramidal cell activity and network function during persistent gamma rhythms. These network changes were associated with specific impairments in hippocampus-dependent spatial working memory and encoding of spatial arrangements and hippocampal-system-related exploratory behavior. The data suggest, therefore, that the recruitment of interneurons into heterogeneous neuronal network activity patterns is correlated with the expression of key aspects of animal behavior.

EXPERIMENTAL PROCEDURES

Generation of Mice Lacking the GluR-D Subunit

The targeting construct was generated from DNA cloned from a 129/SV mouse genomic DNA library. In this construct, a neomycin gene (neo) was placed upstream of exon 11, which encodes for membrane domain 1 and 2 of GluR-D. LoxP sites flanked exon 11 and the neomycin gene. The targeting construct was electroporated into R1 embryonic stem (ES) cells (Nagy et al., 1993). Colonies resistant to G418 were isolated, and positive clones were identified by polymerase chain reaction (PCR) and confirmed by Southern blot. The selection marker cassette was removed in a positive ES cell clone by transient expression of Cre recombinase. Thirteen G418-sensitive clones were identified. Using PCR with a primer set located upstream and downstream of the neo cassette, ES cell clones with a GluR-D^{2lox} allele were identified. The absence of neo and Cre sequences in the genome was confirmed by PCR. One ES clone containing the GluR-D^{2lox} allele was injected into blastocysts of C57/Bl6 mice, and two male chimeras transmitted the GluR-D^{2lox} allele to their offspring. Heterozygous animals of the F1 generation were crossed to CMV-Cre mice (129 and C57BL/6 mixed background) to remove exon 11 from the germ line through Cre/loxP-mediated excision (Nagy et al., 1998). Removal of exon 11 was confirmed by PCR and Southern blot analysis.

Cre Recombinase Expression in PVCre Mice and Generation of *GluR-A^{PVCre-/-}* Mice

The cloning and integration of the PVCre cassette into the translational start of the PV gene of BAC450D23 was carried out as described in (Meyer et al., 2002). Transmission of the transgene was monitored by PCR. The copy number of the integrated transgene was determined via Southern blot analysis after XbaI digestion of genomic DNA and hybridization with a 5' recombogenic arm probe. To characterize Cre recombinase expression, offspring of a founder with a single integrated copy of the Cre transgene were bred to the R26R reporter strain (Soriano, 1999). In the R26R strain, Cre-mediated recombination enables expression of *lacZ*-encoded β -gal. Mice lacking GluR-A expression in PV-positive interneurons were produced by breeding mice carrying a loxP-flanked exon 11 of the GluR-A allele (GluR-A^{2lox}) (Zamanillo et al., 1999) with the PVCre mouse line. Both lines were in a C57Bl/6 genetic background.

Immunohistochemistry

See Supplemental Data.

Electrophysiology

Whole-cell voltage-clamp recordings were performed in transverse hippocampal slices of 250 μ m thickness prepared from the brains of P14 or P42 days old mice. For details see Supplemental Data.

Gamma oscillations were studied in transverse hippocampal slices (450 μ m) prepared from mutant and control animals. For details see Supplemental Data.

Computer Modeling

See Supplemental Data.

Behavioral Analysis

Behavioral testing was done in wt and *GluR-D^{-/-}* male littermates from breeding heterozygous animals backcrossed for four generations to C57BL/6 mice. As controls for the *GluR-A^{PVCre-/-}* mice, littermates positive for the Cre transgene, homozygous for the GluR-A^{2lox} or wt were used. For details on individual behavioral procedures, see Supplemental Data.

Supplemental Data

The Supplemental Data for this article can be found online at <http://www.neuron.org/cgi/content/full/53/4/591/DC1/>.

ACKNOWLEDGMENTS

We thank Drs. P.H. Seeburg and Rolf Sprengel for providing the "floxed" GluR-A mouse line; and Drs. P.H. Seeburg and A. Caputi for their comments on the manuscript and useful discussions; Drs. R-M. Deacon and W.B. Schmitt for help with the behavioral tests; and R. Hinz for technical assistance. This work was supported by the Schilling Foundation, the DFG (FG 577), and the Volkswagenstiftung.

Received: September 6, 2005

Revised: August 28, 2006

Accepted: January 29, 2007

Published: February 14, 2007

REFERENCES

- Alarcon, J.M., Malleret, G., Touzani, K., Vronskaya, S., Ishii, S., Kandel, E.R., and Barco, A. (2004). Chromatin acetylation, memory, and LTP are impaired in CBP+/- mice: a model for the cognitive deficit in Rubinstein-Taybi syndrome and its amelioration. *Neuron* 42, 947-959.
- Angulo, M.C., Lambolez, B., Audinat, E., Hestrin, S., and Rossier, J. (1997). Subunit composition, kinetic, and permeation properties of AMPA receptors in single neocortical nonpyramidal cells. *J. Neurosci.* 17, 6685-6696.
- Bragin, A., Jando, G., Nadasdy, Z., Hetke, J., Wise, K., and Buzsaki, G. (1995). Gamma (40-100 Hz) oscillation in the hippocampus of the behaving rat. *J. Neurosci.* 15, 47-60.
- Burnashev, N., Monyer, H., Seeburg, P.H., and Sakmann, B. (1992). Divalent ion permeability of AMPA receptor channels is dominated by the edited form of a single subunit. *Neuron* 8, 189-198.
- Buzsaki, G. (2002). Theta oscillations in the hippocampus. *Neuron* 33, 325-340.
- Buzsaki, G., Geisler, C., Henze, D.A., and Wang, X.J. (2004). Interneuron diversity series: Circuit complexity and axon wiring economy of cortical interneurons. *Trends Neurosci.* 27, 186-193.
- Catania, M.V., Tolle, T.R., and Monyer, H. (1995). Differential expression of AMPA receptor subunits in NOS-positive neurons of cortex, striatum, and hippocampus. *J. Neurosci.* 15, 7046-7061.
- Catania, M.V., Bellomo, M., Giuffrida, R., Stella, A.M., and Albanese, V. (1998). AMPA receptor subunits are differentially expressed in parvalbumin- and calretinin-positive neurons of the rat hippocampus. *Eur. J. Neurosci.* 10, 3479-3490.
- Celilo, M.R. (1990). Calbindin D-28k and parvalbumin in the rat nervous system. *Neuroscience* 35, 375-475.

- Celio, M.R., Baier, W., Schärer, L., de Viragh, P.A., and Gerday, C. (1988). Monoclonal antibodies directed against the calcium binding protein parvalbumin. *Cell Calcium* 9, 81–86.
- Chrobak, J.J., and Buzsáki, G. (1998). Operational dynamics in the hippocampal-entorhinal axis. *Neurosci. Biobehav. Rev.* 22, 303–310.
- Cobb, S.R., Buhl, E.H., Halasy, K., Paulsen, O., and Somogyi, P. (1995). Synchronization of neuronal activity in hippocampus by individual GABAergic interneurons. *Nature* 378, 75–78.
- Csicsvari, J., Jamieson, B., Wise, K.D., and Buzsáki, G. (2003). Mechanisms of gamma oscillations in the hippocampus of the behaving rat. *Neuron* 37, 311–322.
- DeCoteau, W.E., and Kesner, R.P. (1998). Effects of hippocampal and parietal cortex lesions on the processing of multiple-object scenes. *Behav. Neurosci.* 112, 68–82.
- Engel, A.K., Fries, P., and Singer, W. (2001). Dynamic predictions: oscillations and synchrony in top-down processing. *Nat. Rev. Neurosci.* 2, 704–716.
- Fell, J., Klaver, P., Lehnertz, K., Grunwald, T., Schaller, C., Elger, C.E., and Fernandez, G. (2001). Human memory formation is accompanied by rhinal-hippocampal coupling and decoupling. *Nat. Neurosci.* 4, 1259–1264.
- Fisahn, A., Pike, F.G., Buhl, E.H., and Paulsen, O. (1998). Cholinergic induction of network oscillations at 40 Hz in the hippocampus in vitro. *Nature* 394, 186–189.
- Fortin, N.J., Agster, K.L., and Eichenbaum, H.B. (2002). Critical role of the hippocampus in memory for sequences of events. *Nat. Neurosci.* 5, 458–462.
- Freund, T.F., and Buzsáki, G. (1996). Interneurons of the hippocampus. *Hippocampus* 6, 347–470.
- Geiger, J.R., Melcher, T., Koh, D.S., Sakmann, B., Seeburg, P.H., Jonas, P., and Monyer, H. (1995). Relative abundance of subunit mRNAs determines gating and Ca²⁺ permeability of AMPA receptors in principal neurons and interneurons in rat CNS. *Neuron* 15, 193–204.
- Gilbert, P.E., and Kesner, R.P. (2004). Memory for objects and their locations: the role of the hippocampus in retention of object-place associations. *Neurobiol. Learn. Mem.* 81, 39–45.
- Gloveli, T., Dugladze, T., Saha, S., Monyer, H., Heinemann, U., Traub, R.D., Whittington, M.A., and Buhl, E.H. (2005). Differential involvement of oriens/pyramidal interneurons in hippocampal network oscillations in vitro. *J. Physiol.* 562, 131–147.
- Gray, J. (1982). *The Neuropsychology of Anxiety: An Enquiry into Functions of the Septo-Hippocampal System* (Oxford: Oxford University Press).
- Gray, C.M., König, P., Engel, A.K., and Singer, W. (1989). Oscillatory responses in cat visual cortex exhibit inter-columnar synchronization which reflects global stimulus properties. *Nature* 338, 334–337.
- Honey, R.C., Watt, A., and Good, M. (1998). Hippocampal lesions disrupt an associative mismatch process. *J. Neurosci.* 18, 2226–2230.
- Howard, M.W., Rizzuto, D.S., Caplan, J.B., Madsen, J.R., Lisman, J., Aschenbrenner-Scheibe, R., Schulze-Bonhage, A., and Kahana, M.J. (2003). Gamma oscillations correlate with working memory load in humans. *Cereb. Cortex* 13, 1369–1374.
- Joho, R.H., Ho, C.S., and Marks, G.A. (1999). Increased gamma- and decreased delta-oscillations in a mouse deficient for a potassium channel expressed in fast-spiking interneurons. *J. Neurophysiol.* 82, 1855–1864.
- Jonas, P., Racca, C., Sakmann, B., Seeburg, P.H., and Monyer, H. (1994). Differences in Ca²⁺ permeability of AMPA-type glutamate receptor channels in neocortical neurons caused by differential GluR-B subunit expression. *Neuron* 12, 1281–1289.
- Katsumaru, H., Kosaka, T., Heizmann, C.W., and Hama, K. (1988). Immunocytochemical study of GABAergic neurons containing the calcium-binding protein parvalbumin in the rat hippocampus. *Exp. Brain Res.* 72, 347–362.
- Kawaguchi, Y., and Kubota, Y. (1997). GABAergic cell subtypes and their synaptic connections in rat frontal cortex. *Cereb. Cortex* 7, 476–486.
- Kawaguchi, Y., Katsumaru, H., Kosaka, T., Heizmann, C.W., and Hama, K. (1987). Fast spiking cells in rat hippocampus (CA1 region) contain the calcium-binding protein parvalbumin. *Brain Res.* 416, 369–374.
- Klausberger, T., Roberts, J.D., and Somogyi, P. (2002). Cell type- and input-specific differences in the number and subtypes of synaptic GABA(A) receptors in the hippocampus. *J. Neurosci.* 22, 2513–2521.
- Kondo, M., Sumino, R., and Okado, H. (1997). Combinations of AMPA receptor subunit expression in individual cortical neurons correlate with expression of specific calcium-binding proteins. *J. Neurosci.* 17, 1570–1581.
- Kosaka, T., Katsumaru, H., Hama, K., Wu, J.Y., and Heizmann, C.W. (1987). GABAergic neurons containing the Ca²⁺-binding protein parvalbumin in the rat hippocampus and dentate gyrus. *Brain Res.* 419, 119–130.
- Lambollez, B., Ropert, N., Perrais, D., Rossier, J., and Hestrin, S. (1996). Correlation between kinetics and RNA splicing of alpha-amino-3-hydroxy-5-methylisoxazole-4-propionic acid receptors in neocortical neurons. *Proc. Natl. Acad. Sci. USA* 93, 1797–1802.
- Leranth, C., Szeidemann, Z., Hsu, M., and Buzsáki, G. (1996). AMPA receptors in the rat and primate hippocampus: a possible absence of GluR2/3 subunits in most interneurons. *Neuroscience* 70, 631–652.
- Li, S., Cullen, W.K., Anwyl, R., and Rowan, M.J. (2003). Dopamine-dependent facilitation of LTP induction in hippocampal CA1 by exposure to spatial novelty. *Nat. Neurosci.* 6, 526–531.
- Mann, E.O., Suckling, J.M., Hajos, N., Greenfield, S.A., and Paulsen, O. (2005). Perisomatic feedback inhibition underlies cholinergically induced fast network oscillations in the rat hippocampus in vitro. *Neuron* 45, 105–117.
- Markram, H., Toledo-Rodriguez, M., Wang, Y., Gupta, A., Silberberg, G., and Wu, C. (2004). Interneurons of the neocortical inhibitory system. *Nat. Rev. Neurosci.* 5, 793–807.
- McBain, C.J., and Fisahn, A. (2001). Interneurons unbound. *Nat. Rev. Neurosci.* 2, 11–23.
- Meyer, A.H., Katona, I., Blatow, M., Rozov, A., and Monyer, H. (2002). In vivo labeling of parvalbumin-positive interneurons and analysis of electrical coupling in identified neurons. *J. Neurosci.* 22, 7055–7064.
- Monyer, H., Seeburg, P.H., and Wisden, W. (1991). Glutamate-operated channels: developmentally early and mature forms arise by alternative splicing. *Neuron* 6, 799–810.
- Morris, R.G., Garrud, P., Rawlins, J.N., and O'Keefe, J. (1982). Place navigation impaired in rats with hippocampal lesions. *Nature* 297, 681–683.
- Morris, R.G., Moser, E.I., Riedel, G., Martin, S.J., Sandin, J., Day, M., and O'Carroll, C. (2003). Elements of a neurobiological theory of the hippocampus: the role of activity-dependent synaptic plasticity in memory. *Philos. Trans. R. Soc. Lond. B Biol. Sci.* 358, 773–786.
- Mumby, D.G., Gaskin, S., Glenn, M.J., Schramek, T.E., and Lehmann, H. (2002). Hippocampal damage and exploratory preferences in rats: memory for objects, places, and contexts. *Learn. Mem.* 9, 49–57.
- Nagy, A., Rossant, J., Nagy, R., Abramow-Newerly, W., and Roder, J.C. (1993). Derivation of completely cell culture-derived mice from early-passage embryonic stem cells. *Proc. Natl. Acad. Sci. USA* 90, 8424–8428.
- Nagy, A., Moens, C., Ivanyi, E., Pawling, J., Gertsenstein, M., Hadjantonakis, A.K., Pirity, M., and Rossant, J. (1998). Dissecting the role of N-myc in development using a single targeting vector to generate a series of alleles. *Curr. Biol.* 8, 661–664.

- Nakazawa, K., Quirk, M.C., Chitwood, R.A., Watanabe, M., Yeckel, M.F., Sun, L.D., Kato, A., Carr, C.A., Johnston, D., Wilson, M.A., and Tonegawa, S. (2002). Requirement for hippocampal CA3 NMDA receptors in associative memory recall. *Science* 297, 211–218.
- O'Keefe, J., and Nadel, L. (1978). *The Hippocampus as a Cognitive Map* (Oxford: Oxford University Press).
- Olton, D.S., Becker, J.T., and Handelmann, E. (1979). Hippocampus, space and memory. *Behav. Brain Sci.* 2, 313–366.
- Pawelzik, H., Hughes, D.I., and Thomson, A.M. (2002). Physiological and morphological diversity of immunocytochemically defined parvalbumin- and cholecystokinin-positive interneurons in CA1 of the adult rat hippocampus. *J. Comp. Neurol.* 443, 346–367.
- Pesaran, B., Pezaris, J.S., Sahani, M., Mitra, P.P., and Andersen, R.A. (2002). Temporal structure in neuronal activity during working memory in macaque parietal cortex. *Nat. Neurosci.* 5, 805–811.
- Petralia, R.S., Wang, Y.X., Mayat, E., and Wenthold, R.J. (1997). Glutamate receptor subunit 2-selective antibody shows a differential distribution of calcium-impermeable AMPA receptors among populations of neurons. *J. Comp. Neurol.* 385, 456–476.
- Racca, C., Catania, M.V., Monyer, H., and Sakmann, B. (1996). Expression of AMPA-glutamate receptor B subunit in rat hippocampal GABAergic neurons. *Eur. J. Neurosci.* 8, 1580–1590.
- Rampon, C., Tang, Y.P., Goodhouse, J., Shimizu, E., Kiyin, M., and Tsien, J.Z. (2000). Enrichment induces structural changes and recovery from nonspatial memory deficits in CA1 NMDAR1-knockout mice. *Nat. Neurosci.* 3, 238–244.
- Rawlins, J.N., and Olton, D.S. (1982). The septo-hippocampal system and cognitive mapping. *Behav. Brain Res.* 5, 331–358.
- Reisel, D., Bannerman, D.M., Schmitt, W.B., Deacon, R.M., Flint, J., Borchardt, T., Seeburg, P.H., and Rawlins, J.N. (2002). Spatial memory dissociations in mice lacking GluR1. *Nat. Neurosci.* 5, 868–873.
- Ribak, C.E., Nitsch, R., and Seress, L. (1990). Proportion of parvalbumin-positive basket cells in the GABAergic innervation of pyramidal and granule cells of the rat hippocampal formation. *J. Comp. Neurol.* 300, 449–461.
- Sik, A., Penttonen, M., Ylinen, A., and Buzsaki, G. (1995). Hippocampal CA1 interneurons: an in vivo intracellular labeling study. *J. Neurosci.* 15, 6651–6665.
- Singer, W. (1993). Synchronization of cortical activity and its putative role in information processing and learning. *Annu. Rev. Physiol.* 55, 349–374.
- Solbach, S., and Celio, M.R. (1991). Ontogeny of the calcium binding protein parvalbumin in the rat nervous system. *Anat. Embryol. (Berl.)* 184, 103–124.
- Soriano, P. (1999). Generalized lacZ expression with the ROSA26 Cre reporter strain. *Nat. Genet.* 21, 70–71.
- Soriano, E., Del Rio, J.A., Ferrer, I., Auladell, C., De Lecea, L., and Alcantara, S. (1992). Late appearance of parvalbumin-immunoreactive neurons in the rodent cerebral cortex does not follow an 'inside-out' sequence. *Neurosci. Lett.* 142, 147–150.
- Tallon-Baudry, C., Bertrand, O., and Fischer, C. (2001). Oscillatory synchrony between human extrastriate areas during visual short-term memory maintenance. *J. Neurosci.* 21, RC177.
- Tamas, G., Buhl, E.H., Lorincz, A., and Somogyi, P. (2000). Proximally targeted GABAergic synapses and gap junctions synchronize cortical interneurons. *Nat. Neurosci.* 3, 366–371.
- Tansey, E.P., Chow, A., Rudy, B., and McBain, C.J. (2002). Developmental expression of potassium-channel subunit Kv3.2 within subpopulations of mouse hippocampal inhibitory interneurons. *Hippocampus* 12, 137–148.
- Traub, R.D., Whittington, M.A., Colling, S.B., Buzsaki, G., and Jefferys, J.G. (1996). Analysis of gamma rhythms in the rat hippocampus in vitro and in vivo. *J. Physiol.* 493, 471–484.
- Tsien, J.Z., Huerta, P.T., and Tonegawa, S. (1996). The essential role of hippocampal CA1 NMDA receptor-dependent synaptic plasticity in spatial memory. *Cell* 87, 1327–1338.
- Vinogradova, O.S., and Brazhnik, E.S. (1977). Theta-bursts of hippocampal and septal neurons. *Zh. Vyssh. Nerv. Deiat. Im. I P Pavlova* 27, 1166–1172.
- Vreugdenhil, M., Jefferys, J.G., Celio, M.R., and Schwaller, B. (2003). Parvalbumin-deficiency facilitates repetitive IPSCs and gamma oscillations in the hippocampus. *J. Neurophysiol.* 89, 1414–1422.
- Whittington, M.A., Traub, R.D., and Jefferys, J.G. (1995). Synchronized oscillations in interneuron networks driven by metabotropic glutamate receptor activation. *Nature* 373, 612–615.
- Ylinen, A., Bragin, A., Nadasdy, Z., Jando, G., Szabo, I., Sik, A., and Buzsaki, G. (1995a). Sharp wave-associated high-frequency oscillation (200 Hz) in the intact hippocampus: network and intracellular mechanisms. *J. Neurosci.* 15, 30–46.
- Ylinen, A., Soltesz, I., Bragin, A., Penttonen, M., Sik, A., and Buzsaki, G. (1995b). Intracellular correlates of hippocampal theta rhythm in identified pyramidal cells, granule cells, and basket cells. *Hippocampus* 5, 78–90.
- Yuste, R. (2005). Origin and classification of neocortical interneurons. *Neuron* 48, 524–527.
- Zamanillo, D., Sprengel, R., Hvalby, O., Jensen, V., Burnashev, N., Rozov, A., Kaiser, K.M., Koster, H.J., Borchardt, T., Worley, P., et al. (1999). Importance of AMPA receptors for hippocampal synaptic plasticity but not for spatial learning. *Science* 284, 1805–1811.

Supplemental Data

Recruitment of Parvalbumin-Positive

Interneurons Determines Hippocampal

Function and Associated Behavior

Elke C. Fuchs, Aleksandar R. Zivkovic, Mark O. Cunningham, Steven Middleton, Fiona E.N. LeBeau, David M. Bannerman, Andrei Rozov, Miles A. Whittington, Roger D. Traub, J. Nicholas P. Rawlins, and Hannah Monyer

In situ hybridization. In situ hybridization was performed on coronal sections of adult mice as described in (Monyer et al., 1991)

Immunohistochemistry. WT and transgenic animals were transcardially perfused with 4 % paraformaldehyde; coronal sections were cut at 50 μ m thickness on a vibratome (Leica VT1000S, Heidelberg, Germany) and washed with phosphate buffered saline (PBS). The expression of the GluR-D subunit was analyzed using the avidin-biotin-peroxydase technique (Elite ABC, Vector Laboratories Burlingame, CA). Free-floating slices were cryoprotected by incubation in 30 % sucrose overnight, permeabilized by repeated freezing and thawing over liquid nitrogen; unspecific binding was blocked by 45 min incubation with 5 % bovine serum albumin. After sections were kept at 4° C for 48 hours in PBS with polyclonal glutamate receptor antibody D (1.5 μ g/ml, Chemicon, Temecula, CA), they were rinsed repeatedly with PBS and incubated for 2 hours with 1:400 diluted biotinylated secondary antibody. Sections were washed first with PBS, followed by washing with 20 mM Tris buffer, pH 7.6, incubated for 20 min in Tris buffer containing horseradish-peroxidase-avidin complex (1:500). Peroxidase activity was developed by adding 0.1 % peroxide. Transferring the slices in Tris buffer terminated the reaction. For double labeling the slices were intensively washed with PBS, blocked by 45 min incubation with 5 % bovine serum albumin and kept at 4° C overnight with the monoclonal PV antibody (1:3000, Sigma-Aldrich, Deisenhofen, Germany). Slices

were washed in PBS and incubated for 2 hr with an anti-mouse secondary antibody, conjugated to Cy3 (Jackson Immuno Research, West Grove; PA). After repeated washing with PBS the slices were mounted on 0.1 % gelatin-coated glass slides and mounted in Mowiol 40-88 (Aldrich, Taufkirchen, Germany). Pictures were taken using the BX 51 microscope (Olympus, Japan).

β -galactosidase was performed as previously described (Fuchs et al., 2001). Briefly, free-floating sections were incubated in a X-gal solution containing 5 mM $K_4Fe(CN)_6$, 5 mM $K_3Fe(CN)_6$, 2 mM $MgCl_2$ and 20 mg/ml X-gal in PBS and incubated at 37 °C until the X-gal precipitate was clearly visible. The X-Gal staining was performed prior to immunohistochemical detection of PV with the avidin-biotin-peroxydase technique using the monoclonal parvalbumin antibody (1:3000, Sigma-Aldrich, Deisenhofen, Germany).

Double labeling of GluR-A and PV expression was performed on 50 μ m thick coronal sections that were permeabilized for 30 min in PBS with 0.4 % Triton X-100. This was followed by a preincubation in PBS containing 4 % normal goat serum (NGS). Sections were then incubated overnight at 4° C in PBS containing 0.1 % Triton X-100, 2 % NGS with mouse monoclonal PV antibody (1:3000, Sigma-Aldrich, Deisenhofen, Germany) and polyclonal glutamate receptor A antibody (3 μ g/ml, Chemicon, Temecula, CA). On the following day, slices were washed in PBS and incubated for 2 hr with an anti-mouse secondary antibody, conjugated to Cy3 (Jackson Immuno Research, West Grove; PA), together with an anti-rabbit secondary antibody, conjugated to FITC (Jackson Immuno Research, West Grove; PA). Cells were visualized using immunofluorescence microscopy with appropriate filter sets for Cy3 and FITC.

Biocytin filling and immunostaining. Cells were filled with biocytin (Aldrich, Taufkirchen, Germany; 1-4 mg/ml, dissolved in intercellular solution) during the experiment. Subsequently the slice was fixed overnight in 4 % paraformaldehyde. For double labeling of functionally characterized interneurons, fixed cells were embedded in 4 % agar and resliced in 50 μ m. Slices were transferred in PBS and permeabilized for 30 min in PBS with 0.4 % Triton X-100. This was followed by a preincubation in PBS containing 4 % normal goat serum (NGS). Sections were then incubated overnight at 4° C in PBS containing 0.1 % Triton X-100, 2 %

NGS with mouse monoclonal parvalbumin antibody (1:3000, Sigma-Aldrich, Deisenhofen, Germany), monoclonal calbindin antibody (1:5000, Swant, Bellinzona, Switzerland) or monoclonal somatostatin antibody (1:1000, Chemicon, Temecula, USA). On the following day, slices were washed in PBS and incubated for 2 hr with an anti-mouse secondary antibody, conjugated to Cy3 (Jackson Immuno Research, West Grove; PA), together with FITC-conjugated avidin (Jackson Immuno Research, West Grove; PA) to stain the biocytin-filled cell. Subsequently, slices were mounted in Mowiol, and cells were visualized using immunofluorescence microscopy with appropriate filter sets for Cy3 and FITC.

Electrophysiology. Transverse hippocampal slices of 250 μm thickness were prepared from the brains of P14 or P42 days old mice. Cells were visually identified by infrared differential-contrast video microscopy and by their firing pattern after current injection. Whole-cell voltage clamp recordings were performed in cells that were located in stratum oriens (OLM cells), on the border between stratum oriens and stratum pyramidale (FS cells), in stratum radiatum (CB cells) and stratum pyramidale (PC). Extracellular stimulation was performed with a stimulation pipette filled with extracellular solution. For AMPA/NMDA ratio experiments, the stimulation pipette was positioned in the stratum radiatum of the CA1 region for the recordings of pyramidal and CB cells and in the stratum oriens of the CA1 region, towards the CA3 region, for the recordings of FS and OLM cells. Recording pipettes of 4-6 $\text{M}\Omega$ resistance were filled with intracellular solution containing (in mM): K-gluconate (105), KCl (30), Mg-ATP (4), phosphocreatine (10), GTP (0.3), and HEPES (10), (pH 7.3, 293 mOsm). Extracellular solution contained: (in mM): NaCl (125), KCl (2.5), glucose (25), H_2CO_3 (25), NaH_2PO_4 (1.25), CaCl_2 (2), and MgCl_2 (1). For AMPA/NMDA ratio experiments we used a solution containing 3 mM Ca^{2+} , nominally 0 mM Mg^{2+} , the GABA_A receptor channel blocker bicuculline (BCC, 5 μM) and glycine (10 μM). AMPA and NMDA receptor mediated currents were pharmacologically dissected using AMPA and NMDA receptor channel blockers, CNQX (10 μM) and APV (100 μM), respectively. The holding potential was -70 mV. After recording the total current responses (containing both AMPA and NMDA component, 100 sweeps), AMPA receptor channels were blocked by bath

application of CNQX (10 μ M) and another 100 sweeps containing only NMDA responses were recorded. To confirm that the remaining current after CNQX application was NMDA-mediated; APV (100 μ M) was applied at the end of every experiment. AMPA currents were obtained by subtraction of the averaged NMDA response from the averaged total response and AMPA/NMDA ratios were calculated. Ratios were averaged for each cell type and presented as mean \pm SD. All drugs were purchased from Tocris Bioscience, Ballwin, MO. Stimulus delivery and data acquisition were performed using PULSE software (HEKA Elektronik, Lambrecht, Germany). Analysis was performed using IGOR PRO software (Wavemetrics, Lake Oswego, OR). Firing rates of CA1 FS and pyramidal cells were tested in WT and mutants by rhythmic extracellular stimulation in CA3 stratum pyramidale region. Whole cell current clamp recordings were done simultaneously from a FS cell and an adjacent CA1 pyramidal cell in hippocampal slices (P42). Trains of 9 stimuli (20 Hz) were delivered in CA3 stratum pyramidale region, the stimulus strength and duration was chosen such to be minimal but sufficient to drive firing in both cells. Overall, a stronger stimulus was required to drive firing in the mutants. To compare firing rates between mutants and controls, the stimulation parameters obtained for GluR-D^{-/-} mice (500 μ sec, 10 mA) were used for all genotypes. Experiments were done in presence of bicuculline (5 μ M) to exclude the influence of inhibition. For each cell pair at least 50 sweeps were collected and analysed. Calculation of the statistical significance of differences was performed using unpaired, two-tailed Student's *t* test unless otherwise stated.

Gamma oscillations were studied in transverse hippocampal slices (450 μ m) prepared from mutant and control animals. Mice were anaesthetized with isoflurane, immediately followed by an i.m. injection of ketamine (≥ 100 mg kg⁻¹) and xylazine (≥ 10 mg kg⁻¹). Animals were transcardially perfused with circa 50 ml of modified artificial cerebrospinal fluid (ACSF), which was composed of (in mM): Sucrose (252), KCl (3), NaH₂PO₄ (1.25), NaHCO₃ (24), MgSO₄ (2), CaCl₂ (2) and glucose (10). All salts were obtained from BDH (Poole, UK). The brain was removed and submerged in cold (4-5 °C) ACSF during dissection, and horizontal slices were cut using a vibratome (Leica VT1000S, Heidelberg, Germany). Slices were then transferred to either holding chamber or directly to

recording chamber. Here, they were maintained at 34 °C at the interface between a continuous stream (1.2 ml/min) of ACSF (composition in mM: NaCl (126), KCl (3), NaH₂PO₄ (1.25), NaHCO₃ (24), MgSO₄ (1.25), CaCl₂ (2) and glucose (10)), and warm, moist carbogen gas (95 % O₂ : 5 % CO₂). Slices were permitted to equilibrate for 45 minutes before any recordings commenced. Extracellular recordings electrodes were pulled from borosilicate glass (Harvard Apparatus, UK) filled with ACSF and had resistances in the range of 2~5 MΩ. Intracellular electrodes were pulled from borosilicate glass filled with KCH₃SO₄ and had resistances in the range of 50~100 MΩ. Peak frequency and power values were obtained from power spectra generated with Fourier analysis in the Axograph software package (Axon Instruments, Union City, CA). Power for a given frequency band was determined as the area under the peak in the power spectra between 20 and 80 Hz for gamma frequency oscillations. All values are given as mean ± SEM where normally distributed, otherwise data is expressed as median (Interquartile range). Statistical comparisons were made with repeat measures ANOVA with 'n' corresponding to the number of animals – with a minimum of one slice/neuron analysed per animal. Power spectra were constructed off line from digitised data (digitization frequency 10 kHz) using a 60 second epoch of recorded activity. The kinetics of EPSPs and IPSPs were measured using MiniAnalysis (Synaptosoft, Decatur, GA), >200 IPSPs were obtained per slice and pooled for further analysis.

Computer modeling. We used a model to address the question: does an alteration of interneuron EPSC time course, in a manner determined by experimental data, transform gamma oscillation patterns in a way that also agrees with experiment? If so, alteration of interneuron EPSCs would provide the "minimal explanation" for the observations on persistent gamma oscillations in WT mice and the GluR-D^{-/-} mice. Gamma oscillations in the control ('WT') model are previously described (Traub et al., 2003). The model contains 3072 multicompartiment (axon, soma, branching dendrites) pyramidal cells, and 384 multicompartiment interneurons; the latter population contains axoaxonic cells, basket cells, and dendrite-contacting interneurons. Between cell interactions include synaptic excitation (via AMPA receptors), synaptic inhibition (via

GABA_A receptors), gap junctions between pyramidal cell axons (Schmitz et al., 2001) and gap junctions between interneuron dendrites (Galarreta and Hestrin, 1999; Gibson et al., 1999). The time course of interneuron EPSCs in the control simulation was, in nS, $t \exp(-t)$ (t in ms). For the “GluR-D^{-/-}” simulation, we kept all parameters identical to control, except for the time course of interneuron EPSCs, which became (in nS) $0.09 t \exp(-t/1.5)$. In the results we show the following model data: somatic potentials of pyramidal cells and interneurons, including an interneuron hyperpolarized by -0.75 nA somatic current (to illustrate EPSPs without spikes). We also show a "field", which consists of the inverted average somatic potential of 224 nearby pyramidal cells. Field power spectra were obtained from FFT's of 16,384 data points, representing 3072 ms of data.

For copies of the simulation programs, please contact roger.traub@downstate.edu.

Behavioural analysis. Elevated plus-maze, spontaneous locomotor activity and spatial reference memory on the elevated Y-maze were performed with the same cohort of WT and GluR-D^{-/-} male littermates. The rewarded alternation on the T-maze and tests for object recognition and spatial recognition were done with a different cohort of WT and GluR-D^{-/-} mice. Since in the electrophysiological studies no differences were seen between mice positive for the Cre transgene, homozygous for the GluR-A^{2lox} or WT were seen these genotypes, they were pooled as control mice in the behavioural experiments. Controls consisted of 3 PVCre mice, 9 GluR-A^{2lox/2lox} mice and 6 WT mice.

The test for spatial reference memory on the elevated Y-maze was performed with a new cohort of 9 control (3 WT, 6 GluR-A^{2lox/2lox} mice) and 8 GluR-A^{PVCre^{-/-}} mice.

Elevated plus-maze. The maze was made up of two enclosed arms (27 cm long, 8 cm wide, 30 cm high), painted black, and two open arms (29 cm long, 8 cm wide, with a 0.5 cm high beading; (WT n = 9, GluR-D^{-/-} n = 13 mice). The central junction of the open and the closed arms was a 12.5 x 6 cm rectangle. The apparatus was placed 70 cm above the floor. Mice were placed in an enclosed arm facing the end wall 10 cm away, and were observed for 5 min. The time

spent in the enclosed arms, in the central part, on the open arms and the number of entries into the enclosed arms were recorded.

Automated measurement of spontaneous locomotor activity. Spontaneous locomotor activity was assessed in transparent plastic cages (26 x 16 x 17 cm; WT n = 9, GluR-D^{-/-} n = 13 mice), containing approximately 0.2 cm of sawdust bedding and fitted with ventilated lids. Two horizontal photocell beams were located along the long axis of each cage (1.5 cm above the floor and 14 cm apart). During a 2 hr test session the mice were placed individually into the activity cages and the total number of beam breaks and the number of crossovers (when the front and the back beam were broken consecutively) made by each animal were recorded.

Spatial reference memory in the hidden platform watermaze. The basic protocol has been described elsewhere (Reisel et al., 2002). The performance of 7 WT and 6 GluR-D^{-/-} mice was analyzed; mice exhibiting a high incidence of passive floating (1 WT and 4 GluR-D^{-/-} mice) were excluded. Spatial reference memory was assessed in an open-field water maze, consisting of a large circular tank (diameter 2.0, depth 0.6 m) containing water at 25 ± 1° C to a depth of 0.3 m. To escape from the water, the mice had to find a hidden escape platform (diameter 21 cm) submerged approximately 1 cm below the water surface. The water was made opaque by the addition of 2 liter of milk, which not only prevented the animals from seeing the platform but also allowed efficient tracking of the swim paths. The pool was located on an elevated platform 60 cm above the floor in another new, well-lit laboratory containing prominent extramaze cues. Swim paths were monitored by a video camera mounted in the ceiling. Mouse position was tracked by computer (HVS VP112, HVS Image, Hampton, UK). The platform was located at the centre of one of four quadrants of the pool (arbitrarily designated NE, NW, SE and SW). The number of mice trained to each platform position was counterbalanced with respect to group. Animals had no swim pretraining before the start of spatial testing in the water maze. All mice were trained to find a hidden platform, which remained in a fixed location throughout testing. They received 4 trials per day for 9 days, with an inter-trial interval (ITI) of approximately 15 s. The mice were placed into the

pool facing the sidewall at one of 8 start locations (nominally N, S, E, W, NE, NW, SE and SW; chosen randomly across trials), and allowed to swim until they found the platform, or for a maximum of 90 s. Any mouse that failed to find the platform within the allowed time was lifted out of the water by the experimenter and placed onto the platform. The animal then remained on the platform for 30 s before commencing the next trial.

On the tenth day of testing (24 h after spatial training trial 36), a probe trial was conducted to determine the extent to which the mice had learned about the spatial location of the platform. The platform was removed from the pool, and the mice were allowed to swim freely for 90 s. The percentage of time that animals spent in each quadrant of the maze was recorded.

Spatial reference memory on the elevated Y-maze. Mice were maintained on a restricted feeding schedule at 85 % of their free-feeding weight. Spatial reference memory was examined using an elevated Y-maze made of black painted wood. It had a central polygonal area 14 cm in diameter to which three arms were attached (50 x 9 cm, surrounded by a 0.5 cm high beading). A metal food well was located 5 cm from the distal end of each arm. The maze was located in a new laboratory with prominent distal cues, and was elevated 80 cm above the ground on a central stand on which the entire maze could be rotated to prevent the use of intra-maze cues. Mice were familiarized to the maze until they were running freely on the maze and readily consuming milk rewards from the food wells in the holding room. Spatial reference memory testing was performed in a different room. A target arm (defined according to its given spatial location relative to the room cues) was designated for each mouse to receive 0.1 ml reward of sweetened, condensed milk (diluted 50/50 with water). Target arms were counterbalanced with respect to group such that approximately equal numbers of mutant and WT animals were trained to each of the arms. The start arm for each trial was determined by a pseudorandom sequence with equal numbers of starts from each arm in any one session, and no more than three consecutive starts from the same arm: see (Reisel et al., 2002).

Spatial working memory on the elevated T-maze. Mice were maintained on a restricted feeding schedule at 85 % of their free-feeding weight. Spatial working

memory was assessed on an elevated wooden T-maze. This consisted of a start arm (47 x 10 cm) and two identical goal arms (35 x 10 cm), surrounded by a 10 cm high wall. A metal food well was located 3 cm from the end of each goal arm. The maze was located 1 m above the floor in a well-lit laboratory that contained various prominent distal extramaze cues. The mice were habituated to the maze, and to drinking sweetened, condensed milk, over several days before spatial non-matching-to-place testing. Each trial consisted of a sample run and a choice run. On the sample run, the mice were forced either left or right by the presence of a wooden block, according to a pseudorandom sequence (with equal numbers of left and right turns per session, and with not more than two consecutive turns in the same direction). A reward consisting of 0.1 ml of milk was available in the food well at the end of the arm. The time interval between the sample run and the choice run was approximately 15 s. The animal was rewarded for choosing the previously unvisited arm (that is, for alternating). Mice were run one trial at a time with an ITI (inter-trial interval) of approximately 10 min. Each daily session consisted of 2 to 3 trials, and mice received 40 trials in total.

Open field. The open field consisted of a gray PVC enclosed arena (50 x 30 x 18 cm), which was divided into 10 x 10 cm squares. Since our aim was to assess activity and exploration, and not to subject the mice to a strongly anxiogenic situation, normal room illumination was used. Mice were placed individually into one corner of the maze facing the sidewalls and observed for 3 min. The total number of squares crossed, latency to move, total number of rears, and latency to first rear were recorded. Two consecutive tests were run.

Novel object recognition tasks. Mice were individually habituated to an open field box (50 x 30 x 18 cm) for 3 days. During the training session, two different objects X and Y (task 1) or two identical objects X1 and X2 (task 2) were placed into the open field and the mouse was allowed to explore for 5 min. The time spent exploring each object was recorded. After a 5 min break during the test phase the animals were placed back into the same box, in which one of the familiar objects was replaced by a novel object Y, and allowed to explore freely for 5 min. A camcorder was used to evaluate the performance of the animals on a computer screen by an observer blind to the genotype of the animals. The time

exploring the familiar and the new object was recorded; a duplicate of the original familiar object was used to avoid the use of odour cues. The time spent with the new object compared with the time spent with the familiar object during the retention test was used to measure recognition memory. All objects presented were of similar surface structures and sizes, but had distinctive shapes and colours and the objects were presented in a counterbalanced order to prevent spontaneous object preference.

Spatial recognition task. The mice were exposed to four successive 5 min sessions in an open field box (with a 5 min inter-trial interval). During the first session the mice are habituated to the empty arena, in the two following sessions the animals are allowed to explore three different objects (X, Y and Z). A camcorder was used to evaluate the performance of the animals on a computer screen by an observer blind to the genotype of the animals. The time spent exploring each object was recorded. In between the sessions the mouse was placed back into the home cage. During the test phase, one object was moved to a different location thereby altering the spatial arrangement of the arena. The amount of time spent exploring the object with changed position (test session) compared with the time spent exploring the two other objects, was used to measure spatial recognition memory. Triplicates of each object were used to avoid the use of odour cues. All objects presented were of similar surface structures and sizes, but distinctive shapes and colours and the objects were presented in a counterbalanced order to prevent spontaneous object preference.

Data analysis for behavioural analysis. Parametric data are presented as means (\pm SEM), and were analyzed by *t*-test and ANOVA followed by the Newman-Keuls *post hoc* analysis. Non-parametric data are represented as medians (\pm IQR), and were analyzed by the Kruskal-Wallis one way analysis of variance on ranks and the Mann-Whitney rank sum test.

References

Fuchs, E. C., Doheny, H., Faulkner, H., Caputi, A., Traub, R. D., Bibbig, A., Kopell, N., Whittington, M. A., and Monyer, H. (2001). Genetically altered AMPA-type

glutamate receptor kinetics in interneurons disrupt long-range synchrony of gamma oscillation. *Proc Natl Acad Sci U S A* *98*, 3571-3576.

Galarreta, M., and Hestrin, S. (1999). A network of fast-spiking cells in the neocortex connected by electrical synapses. *Nature* *402*, 72-75.

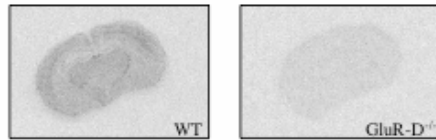
Gibson, J. R., Beierlein, M., and Connors, B. W. (1999). Two networks of electrically coupled inhibitory neurons in neocortex. *Nature* *402*, 75-79.

Monyer, H., Seeburg, P. H., and Wisden, W. (1991). Glutamate-operated channels: developmentally early and mature forms arise by alternative splicing. *Neuron* *6*, 799-810.

Reisel, D., Bannerman, D. M., Schmitt, W. B., Deacon, R. M., Flint, J., Borchardt, T., Seeburg, P. H., and Rawlins, J. N. (2002). Spatial memory dissociations in mice lacking GluR1. *Nat Neurosci* *5*, 868-873.

Schmitz, D., Schuchmann, S., Fisahn, A., Draguhn, A., Buhl, E. H., Petrasch-Parwez, E., Dermietzel, R., Heinemann, U., and Traub, R. D. (2001). Axo-axonal coupling: a novel mechanism for ultrafast neuronal communication. *Neuron* *31*, 831-840.

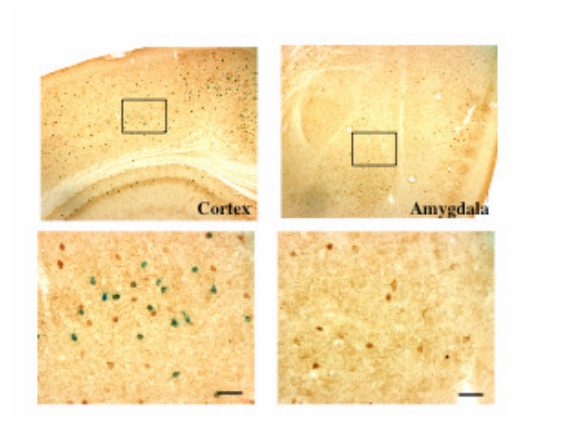
Traub, R. D., Cunningham, M. O., Gloveli, T., LeBeau, F. E., Bibbig, A., Buhl, E. H., and Whittington, M. A. (2003). GABA-enhanced collective behavior in neuronal axons underlies persistent gamma-frequency oscillations. *Proc Natl Acad Sci U S A* *100*, 11047-11052.



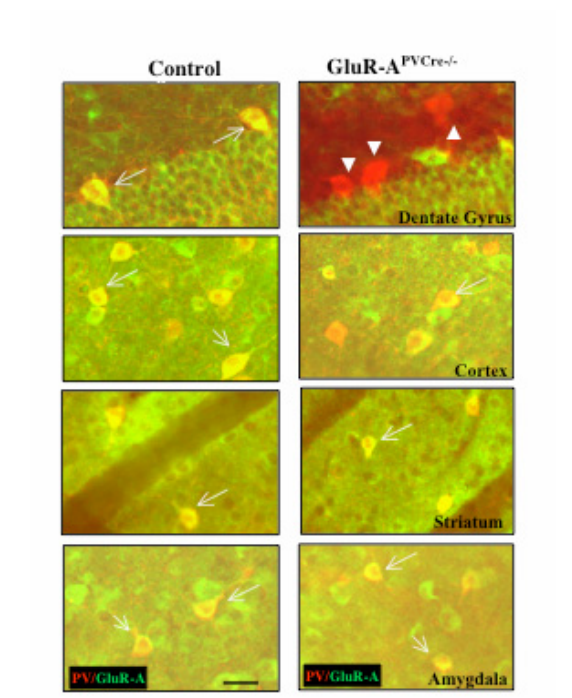
Supplemental Figure S1. mRNA expression in WT and GluR-D^{-/-} mice

X-ray autoradiography showing GluR-D transcript expression in coronal brain section of Adult WT and GluR-D^{-/-} siblings demonstrating the lack of expression in the knockout.

A



B

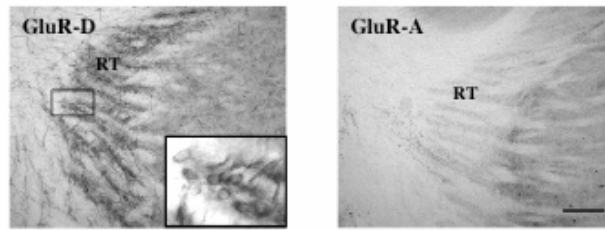


Brain region	% Pv cells without GluR-A expression	Number of cells analyzed
RSG cortex	97 ± 0.96	521
S1BF cortex	76 ± 6	581
Perirhinal cortex	3.25 ± 1.7	317
Striatum	26 ± 10.5	124
Basolateral amygdala	5.25 ± 1.25	187
Hippocampus		
Dentate gyrus	93 ± 3.75	105
CA3	93 ± 2	154
CA1	98 ± 2	108

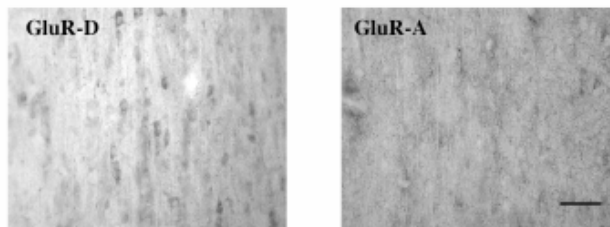
Supplemental Figure S2. Cre-recombinase expression in PV-positive interneurons of the hippocampus and in other brain regions

(A) Recombination of the R26R reporter in selected brain regions. Upper panels show lower magnification of the cortex and amygdala. Boxes indicate the regions which are shown at a higher magnification in the lower panels. Co-labeling of PV (brown) with X-gal staining (blue) occurs only in a subset of PV-positive cells in the cortex. There is no detectable Cre recombinase activity in the amygdala. Scale bars are 50 μ m. (B) Cre-mediated excision of exon 11 of the GluR-A gene is more efficient in the hippocampus vs. other brain regions. Double-labeling for PV (red) and GluR-A (green) expression reveals the absence of GluR-A in most PV-positive cells in the dentate gyrus in the hippocampus of GluR-A^{PVCre-/-} mice, comparable to the cell-type specific ablation already described for the CA1 region (Figure 1). In certain cortical regions, striatum and amygdala, the majority of PV-positive cells still express GluR-A in GluR-A^{PVCre-/-} mice. Arrows indicate PV/GluR-A positive cells, arrow heads indicate PV-positive cells in the dentate gyrus after deletion of GluR-A. Scale bars are 30 μ m. For quantitative evaluation see table below. Coronal sections from 4 GluR-A^{PVCre-/-} were analyzed and the percentage of PV-positive cells without GluR-A expression calculated. The comparison with the PV- and GluR-A double-positive cells in coronal slices from 4 control animals (data not shown) revealed that the loss of the GluR-A subunit did not lead to obvious changes in the pattern and number of PV-positive cells in adult GluR-A^{PVCre-/-} mice. Abbreviation, RSG, retrosplenial granular cortex; S1BF, somatosensory cortex, barrel field.

A

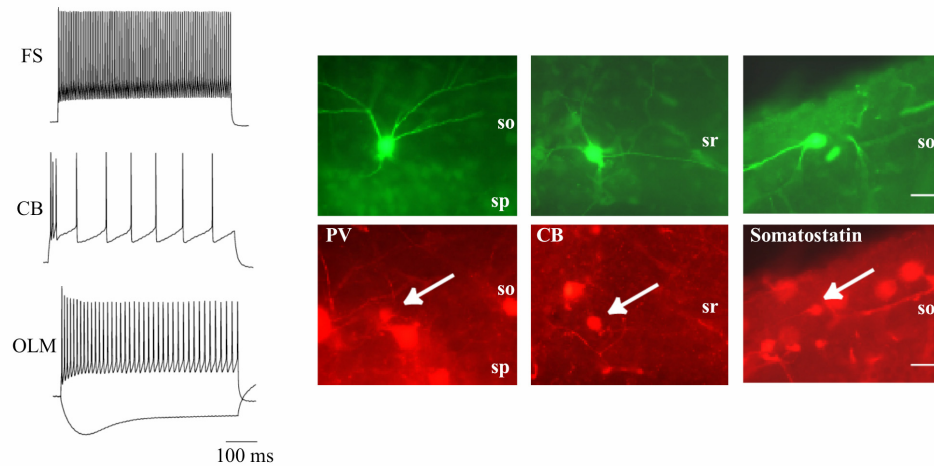


B



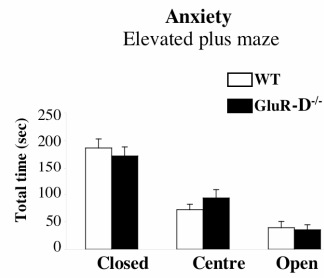
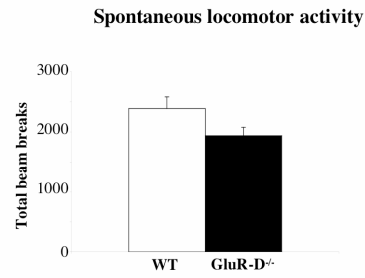
Supplemental Figure S3. GluR-D expression in interneurons of the reticular thalamus and medial septum

(A) Immunocytochemistry demonstrates significant levels of GluR-D but not GluR-A expression in interneurons of the reticular thalamus (Scale bar is 150 μ m) and (B) medial septum (Scale bar is 100 μ m. Abbreviation, RT, reticular thalamus).



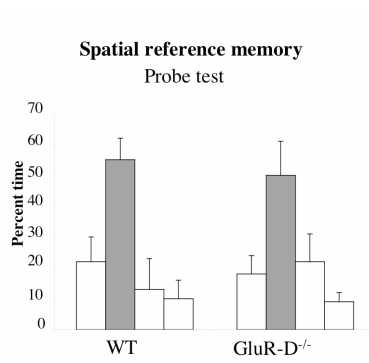
Supplemental Figure S4. Identification of different subpopulations of interneurons in the CA1 region of the hippocampus

Interneurons were identified by location, shape of cell body and firing pattern of action potentials upon current injection (left panel). FS cells are characterized by a non-accommodating, non-attenuating and high frequency firing pattern. The pattern for CB-positive cells was characterized by an initial burst of three APs followed by a regular spiking pattern at lower frequency. Injection of hyperpolarizing current into OLM cells results in the typical ‘sag’ of the initial current segment while depolarizing current injection generates a train of APs that decrease in amplitude and slightly also in frequency. The identity of the three cell types was subsequently confirmed by biocytin filling (right upper panels) and immunostaining for PV, CB and somatostatin (right lower panels), as indicated by white arrows. In WT 7 out of 7 cells were positive for PV, 5 out of 5 cells were positive for CB and 7 out of 7 cells were positive for somatostatin. In *GluR-D^{-/-}* mice 7 out of 7 cells were positive for PV. Scale bars are 20 μm ; so, stratum oriens; sp, stratum pyramidale; sr, stratum radiatum.

A**B**

Supplemental Figure S5. Unaltered anxiety and spontaneous locomotor activity in GluR-D^{-/-} mice

(A) Both the WT and GluR-D^{-/-} mice performed similarly on the elevated plus maze; they spent a comparable amount of time in the closed or open arms and in the central part of the plus maze. (B) No significant differences between WT and GluR-D^{-/-} mice were observed during the assessment of spontaneous locomotor activity measured as total number of beam breaks of two light beams in photocell activity cages (WT n = 9, GluR-D^{-/-} n = 13 mice).



Supplemental Figure S6. Unaltered spatial reference memory in GluR-D^{-/-} mice
Standard spatial reference memory version of the Morris watermaze task. Mean percent of time spent in the four quadrants of the pool during the 90 s probe test, conducted at the end of spatial training (after 36 trials). The platform had previously been located in the training quadrant (solid gray bars) during acquisition (WT n = 7, GluR-D^{-/-} n = 6 mice).